

# Chargino and neutralino production at $e^+e^-$ colliders in the complex MSSM: a full one-loop analysis

S. Heinemeyer<sup>1,2,3,a</sup>, C. Schappacher<sup>4,b</sup>

<sup>1</sup> Campus of International Excellence UAM+CSIC, Cantoblanco, 28049 Madrid, Spain

<sup>2</sup> Instituto de Física Teórica (UAM/CSIC), Universidad Autónoma de Madrid, Cantoblanco, 28049 Madrid, Spain

<sup>3</sup> Instituto de Física de Cantabria (CSIC-UC), 39005 Santander, Spain

<sup>4</sup> Emil-Goett-Str. 27, D-76131 Karlsruhe, Germany

Received: 3 May 2017 / Accepted: 5 September 2017 / Published online: 26 September 2017  
© The Author(s) 2017. This article is an open access publication

**Abstract** For the search for charginos and neutralinos in the Minimal Supersymmetric Standard Model (MSSM) as well as for future precision analyses of these particles an accurate knowledge of their production and decay properties is mandatory. We evaluate the cross sections for the chargino and neutralino production at  $e^+e^-$  colliders in the MSSM with complex parameters (cMSSM). The evaluation is based on a full one-loop calculation of the production mechanisms  $e^+e^- \rightarrow \tilde{\chi}_c^\pm \tilde{\chi}_c^\mp$  and  $e^+e^- \rightarrow \tilde{\chi}_n^0 \tilde{\chi}_n^0$  including soft and hard photon radiation. We mostly restricted ourselves to a version of our renormalization scheme which is valid for  $|M_1| < |M_2|$ ,  $|\mu|$  and  $M_2 \neq \mu$  to simplify the analysis, even though we are able to switch to other parameter regions and correspondingly different renormalization schemes. The dependence of the chargino/neutralino cross sections on the relevant cMSSM parameters is analyzed numerically. We find sizable contributions to many production cross sections. They amount to roughly  $\pm 15\%$  of the tree-level results but can go up to  $\pm 40\%$  or higher in extreme cases. Also the complex phase dependence of the one-loop corrections was found non-negligible. The full one-loop contributions are thus crucial for physics analyses at a future linear  $e^+e^-$  collider such as the ILC or CLIC.

## 1 Introduction

One of the important tasks at the LHC is to search for physics beyond the Standard Model (SM), where the Minimal Supersymmetric Standard Model (MSSM) [1–4] is one of the lead-

ing candidates. Two related important tasks are the investigation of the mechanism of electroweak symmetry breaking, including the identification of the underlying physics of the Higgs boson discovered at  $\sim 125$  GeV [5,6], as well as the production and measurement of the properties of Cold Dark Matter (CDM). Here the MSSM offers a natural candidate for CDM, the Lightest Supersymmetric Particle (LSP), the lightest neutralino,  $\tilde{\chi}_1^0$  [7,8] (see below). These three (related) tasks will be the top priority in the future program of particle physics.

Supersymmetry (SUSY) predicts two scalar partners for all SM fermions as well as fermionic partners to all SM bosons. Contrary to the case of the SM, in the MSSM two Higgs doublets are required. This results in five physical Higgs bosons instead of the single Higgs boson in the SM. These are the light and heavy  $\mathcal{CP}$ -even Higgs bosons,  $h$  and  $H$ , the  $\mathcal{CP}$ -odd Higgs boson,  $A$ , and the charged Higgs bosons,  $H^\pm$ . In the MSSM with complex parameters (cMSSM) the three neutral Higgs bosons mix [9–13], giving rise to the  $\mathcal{CP}$ -mixed states  $h_1, h_2, h_3$ . The neutral SUSY partners of the (neutral) Higgs and electroweak gauge bosons are the four neutralinos,  $\tilde{\chi}_{1,2,3,4}^0$ . The corresponding charged SUSY partners are the charginos,  $\tilde{\chi}_{1,2}^\pm$ .

If SUSY is realized in nature and the scalar quarks and/or the gluino are in the kinematic reach of the LHC, it is expected that these strongly interacting particles are copiously produced. On the other hand, SUSY particles that interact only via the electroweak force, e.g., the charginos and neutralinos, have a much smaller production cross section at the LHC. Correspondingly, the LHC discovery potential as well as the current experimental bounds are substantially weaker (and no charginos or neutralinos have been discovered yet).

At a (future)  $e^+e^-$  collider charginos and neutralinos, depending on their masses and the available center-of-mass energy, could be produced and analyzed in detail. Corre-

Former address of author C. Schappacher—Institut für Theoretische Physik, Karlsruhe Institute of Technology, 76128 Karlsruhe, Germany.

<sup>a</sup> e-mail: [Sven.Heinemeyer@cern.ch](mailto:Sven.Heinemeyer@cern.ch)

<sup>b</sup> e-mail: [schappacher@kabelbw.de](mailto:schappacher@kabelbw.de)

sponding studies can be found for the ILC in Refs. [14–19] and for CLIC in Refs. [19–21]. (Results on the combination of LHC and ILC results can be found in Refs. [22–24].) Such precision studies will be crucial to determine their nature and the underlying (SUSY) parameters.

In order to yield a sufficient accuracy, one-loop corrections to the various chargino/neutralino production and decay modes have to be considered. Full one-loop calculations in the cMSSM for various chargino/neutralino decays in the cMSSM have been presented over the last years [25–28]. One-loop corrections for their production from the decay of Higgs bosons (at the LHC or ILC/CLIC) can be found in Ref. [29]. In this paper we take the next step and concentrate on the chargino/neutralino production at  $e^+e^-$  colliders, i.e. we calculate,

$$\sigma(e^+e^- \rightarrow \tilde{\chi}_c^\pm \tilde{\chi}_{c'}^\mp) \quad (c, c' = 1, 2), \quad (1)$$

$$\sigma(e^+e^- \rightarrow \tilde{\chi}_n^0 \tilde{\chi}_{n'}^0) \quad (n, n' = 1, 2, 3, 4). \quad (2)$$

Our evaluation of the two channels (1) and (2) is based on a full one-loop calculation, i.e. including electroweak (EW) corrections, as well as soft and hard QED radiation. The renormalization scheme employed is the same one as for the decay of charginos/neutralinos [25–28]. Consequently, the predictions for the production and decay can be used together in a consistent manner.

Results for the cross sections (1) and (2) at various levels of sophistication have been obtained over the last three decades. Tree-level results were published for  $e^+e^- \rightarrow \tilde{\chi}_c^\pm \tilde{\chi}_{c'}^\mp$  and  $e^+e^- \rightarrow \tilde{\chi}_n^0 \tilde{\chi}_{n'}^0$  in the MSSM with real parameters (rMSSM) in Refs. [30,31]. Tree-level results for the cMSSM for  $e^+e^- \rightarrow \tilde{\chi}_n^0 \tilde{\chi}_{n'}^0$  (using a “projector formalism”) were presented in Ref. [32]. Results for  $\mathcal{CP}$ -odd observables with  $e^+e^- \rightarrow \tilde{\chi}_c^\pm \tilde{\chi}_{c'}^\mp$  ( $c \neq c'$ ) were shown in Ref. [33] (including “selected box contributions”) and extended to the full contributions in Refs. [34,35]. Vertex corrections to  $e^+e^- \rightarrow \tilde{\chi}_c^\pm \tilde{\chi}_{c'}^\mp$  in the rMSSM including the contributions of  $t/\tilde{t}/b/\tilde{b}$  were evaluated in Ref. [36], using an  $\overline{\text{MS}}$  renormalization scheme. The results including all quark/squark contributions were shown in Ref. [37] (claiming differences to Ref. [36]). Full one-loop corrections in the rMSSM for  $e^+e^- \rightarrow \tilde{\chi}_c^\pm \tilde{\chi}_{c'}^\mp$  were first presented in Ref. [38] and later in Ref. [39]. The  $\tilde{\chi}_1^0 \tilde{\chi}_1^0$  production together with a photon was analyzed in Refs. [40,41]. The inclusion of multi-photon emission and the implementation into an event generator was presented in Refs. [42,43].  $e^+e^- \rightarrow \tilde{\chi}_n^0 \tilde{\chi}_{n'}^0$  and  $e^+e^- \rightarrow \tilde{\chi}_c^\pm \tilde{\chi}_{c'}^\mp$  were calculated at the full one-loop level in the rMSSM in Ref. [44], and later also in Ref. [45] (but without including a numerical analysis). Full one-loop results for  $e^+e^- \rightarrow \tilde{\chi}_n^0 \tilde{\chi}_{n'}^0$  in the rMSSM were shown in Ref. [46], where the soft SUSY-breaking parameter  $M_2$  and the Higgs mixing parameter  $\mu$  were renormalized on-shell (and only results for  $e^+e^- \rightarrow$

$\tilde{\chi}_1^0 \tilde{\chi}_2^0$  and  $e^+e^- \rightarrow \tilde{\chi}_2^0 \tilde{\chi}_2^0$  were analyzed numerically). The latter results were extended to  $e^+e^- \rightarrow \tilde{\chi}_n^0 \tilde{\chi}_{n'}^0$  and  $e^+e^- \rightarrow \tilde{\chi}_c^\pm \tilde{\chi}_{c'}^\mp$  in the cMSSM in Ref. [47], but only real parameters have been considered. Subsequently, full one-loop results in the cMSSM for  $e^+e^- \rightarrow \tilde{\chi}_n^0 \tilde{\chi}_{n'}^0$  and  $e^+e^- \rightarrow \tilde{\chi}_c^\pm \tilde{\chi}_{c'}^\mp$  were obtained in Refs. [48–51], but only real parameters were included in the phenomenological analysis. Finally, in Ref. [52] the effects of imaginary and absorptive parts have been analyzed for  $e^+e^- \rightarrow \tilde{\chi}_c^\pm \tilde{\chi}_{c'}^\mp$ , and for a precise cMSSM parameter extraction from experiment, full one-loop corrections to  $e^+e^- \rightarrow \tilde{\chi}_n^0 \tilde{\chi}_{n'}^0$  and  $e^+e^- \rightarrow \tilde{\chi}_c^\pm \tilde{\chi}_{c'}^\mp$  were presented (for three benchmark points) in Ref. [53]. The differences in our renormalization in the chargino/neutralino sector from the previous two papers are discussed in our Ref. [27].

In this paper we present for the first time a full and consistent one-loop calculation in the cMSSM for chargino and neutralino production at  $e^+e^-$  colliders. We take into account soft and hard QED radiation and the treatment of collinear divergences. Again, here it is crucial to stress that the same renormalization scheme as for the decay of charginos/neutralinos [25–28] (and for the production of charginos/neutralinos from Higgs-boson decays [29]) has been used. Consequently, the predictions for the production and decay can be used together in a consistent manner (e.g., in a global phenomenological analysis of the chargino/neutralino sector at the one-loop level). We analyze all processes w.r.t. the most relevant parameters, including the relevant complex phases. In this way we go substantially beyond the existing analyses (see above). In Sect. 2 we very briefly review the renormalization of the relevant sectors of the cMSSM and give details as regards the calculation. In Sect. 3 various comparisons with results from other groups are given. The numerical results for the production channels (1) and (2) are presented in Sect. 4. The conclusions can be found in Sect. 5.

## Prolegomena

We use the following short-hands in this paper:

- FeynTools  $\equiv$  FeynArts + FormCalc + LoopTools.
- full = tree + loop.
- $s_w \equiv \sin \theta_w$ ,  $c_w \equiv \cos \theta_w$ .
- $t_\beta \equiv \tan \beta$ .

They will be further explained in the text below.

## 2 Calculation of diagrams

In this section we give some details regarding the renormalization procedure and the calculation of the tree-level

and higher-order corrections to the production of charginos and neutralinos in  $e^+e^-$  collisions. The diagrams and corresponding amplitudes have been obtained with `FeynArts` (version 3.9) [54–57], using the MSSM model file (including the MSSM counterterms) of Ref. [58]. The further evaluation has been performed with `FormCalc` (version 9.5) and `LoopTools` (version 2.13) [59,60].

### 2.1 The complex MSSM

The cross sections (1) and (2) are calculated at the one-loop level, including soft and hard QED radiation; see the next section. This requires the simultaneous renormalization of the gauge-boson sector, the fermion/sfermion sector as well as the chargino/neutralino sector of the cMSSM. We give a few relevant details as regards these sectors and their renormalization. More details and the application to Higgs-boson and SUSY particle decays can be found in Refs. [25–29,58,61–66]. Similarly, the application to Higgs-boson production cross sections at  $e^+e^-$  colliders are given in Refs. [67,68].

The renormalization of the fermion/sfermion and gauge-boson sectors follows strictly Ref. [58] and the references therein (see especially Ref. [69]). This defines in particular the counterterm  $\delta t_\beta$ , as well as the counterterms for the  $Z$  boson mass,  $\delta M_Z^2$ , and for the sine of the Weinberg mixing angle,  $\delta s_w$  (with  $s_w = \sqrt{1 - c_w^2} = \sqrt{1 - M_W^2/M_Z^2}$ , where  $M_W$  and  $M_Z$  denote the  $W$  and  $Z$  boson masses, respectively).

For the fermion sector we use the default values as given in Ref. [58]. In the slepton sector we use the on-shell (OS) scheme OS [1], i.e. in the notation of [58]<sup>1</sup>:

`$SfScheme[2, g] = OS[1]`  
 on-shell scheme with  $m_{\tilde{e}_L}$  OS,  $Y_{e_g}$  OS.

The chargino/neutralino sector is also described in detail in Ref. [58] and the references therein; see in particular Refs. [25–28,64]. In this paper we use mostly the CCN [1] scheme (i.e. OS conditions for the two charginos and the lightest neutralino), as implemented in the `FeynArts` model file `MSSMCT.mod` [58]. Also some CNN [ $c, n, n'$ ] schemes (OS conditions for one chargino and two neutralinos, as implemented in `MSSMCT.mod`) have been used for a few comparative calculations, as will be detailed below. Either scheme fixes three out of six chargino/neutralino masses to be on-shell. The other three masses then acquire a finite shift. The one-loop masses of the remaining charginos/neutralinos are obtained from the tree-level ones via the shifts [70,71]:

$$\Delta m_{\tilde{\chi}_c^\pm} = -\text{Re} \left\{ m_{\tilde{\chi}_c^\pm} \left( \Sigma_{\tilde{\chi}_c^\pm}^L(m_{\tilde{\chi}_c^\pm}^2) + \frac{1}{2} [\delta \mathbf{Z}_{\tilde{\chi}_c^\pm}^L + \delta \check{\mathbf{Z}}_{\tilde{\chi}_c^\pm}^L]_{cc} \right) + \Sigma_{\tilde{\chi}_c^\pm}^{SL}(m_{\tilde{\chi}_c^\pm}^2) - \frac{1}{2} m_{\tilde{\chi}_c^\pm} [\delta \mathbf{Z}_{\tilde{\chi}_c^\pm}^R + \delta \check{\mathbf{Z}}_{\tilde{\chi}_c^\pm}^R]_{cc} - [\delta \mathbf{M}_{\tilde{\chi}_c^\pm}]_{cc} \right\}, \tag{3}$$

$$\Delta m_{\tilde{\chi}_n^0} = -\text{Re} \left\{ m_{\tilde{\chi}_n^0} \left( \Sigma_{\tilde{\chi}_n^0}^L(m_{\tilde{\chi}_n^0}^2) + \frac{1}{2} [\delta \mathbf{Z}_{\tilde{\chi}_n^0}^R + \delta \check{\mathbf{Z}}_{\tilde{\chi}_n^0}^R]_{nn} \right) + \Sigma_{\tilde{\chi}_n^0}^{SL}(m_{\tilde{\chi}_n^0}^2) - \frac{1}{2} m_{\tilde{\chi}_n^0} [\delta \mathbf{Z}_{\tilde{\chi}_n^0}^L + \delta \check{\mathbf{Z}}_{\tilde{\chi}_n^0}^L]_{nn} - [\delta \mathbf{M}_{\tilde{\chi}_n^0}]_{nn} \right\} \tag{4}$$

with  $c = 1, 2; n = 1, 2, 3, 4$ , where  $\Sigma_{\tilde{\chi}}^{(S)L}(p^2 = m_{\tilde{\chi}}^2)$  denotes the unrenormalized (scalar) left-handed part of the fermionic self-energy. The field renormalization constants  $\delta \mathbf{Z}$  (including absorptive parts for incoming  $\delta \check{\mathbf{Z}}$  and outgoing  $\delta \check{\mathbf{Z}}$  particles) and the mass renormalization constants  $\delta \mathbf{M}$  can be found in Section 3.4 of Ref. [58]. For all externally appearing chargino/neutralino masses the (shifted) “on-shell” masses are used:

$$m_{\tilde{\chi}_c^\pm}^{\text{OS}} = m_{\tilde{\chi}_c^\pm} + \Delta m_{\tilde{\chi}_c^\pm}, \quad m_{\tilde{\chi}_n^0}^{\text{OS}} = m_{\tilde{\chi}_n^0} + \Delta m_{\tilde{\chi}_n^0}. \tag{5}$$

In order to yield UV-finite results the tree-level values  $m_{\tilde{\chi}_c^\pm}$  and/or  $m_{\tilde{\chi}_n^0}$  for all internally appearing chargino/neutralino masses in loop calculations are used. Renormalizing the two charged states OS (as done in CCN schemes), i.e. ensuring that they have the same mass at the tree- and at the loop level is (in general) crucial for the cancellation of the IR divergencies. On the other hand, CNN schemes are IR divergent if an externally appearing chargino is not chosen OS.

The CCN [1] scheme defines in particular the counterterm  $\delta \mu$ , where  $\mu$  denotes the Higgs mixing parameter. This scheme yields numerically stable results for  $|M_1| < |M_2|$ ,  $|\mu|$  and  $M_2 \neq \mu$ , i.e. the lightest neutralino is bino-like and defines the counterterm for  $M_1$  [25–28,72]. In the numerical analysis this mass pattern holds. Switching to a different mass pattern, e.g., with  $|M_2| < |M_1|$  and/or  $M_2 \sim \mu$  requires one to switch to a different renormalization scheme [58,72]. While these schemes are implemented into the `FeynArts/FormCalc` framework [58], so far no automated choice of the renormalization scheme has been devised. For simplicity we stick (mostly) to the CCN [1] scheme with a matching choice of SUSY parameters; see Sect. 4.1.

### 2.2 Contributing diagrams

Sample diagrams for the process  $e^+e^- \rightarrow \tilde{\chi}_c^\pm \tilde{\chi}_c^\mp$  are shown in Fig. 1 and for the process  $e^+e^- \rightarrow \tilde{\chi}_n^0 \tilde{\chi}_{n'}^0$  in Fig. 2. Not shown are the diagrams for real (hard and soft) photon radi-

<sup>1</sup> Accidentally, for our parameter set (see Table 2) the renormalization scheme OS [2] leads to unacceptable large loop corrections.

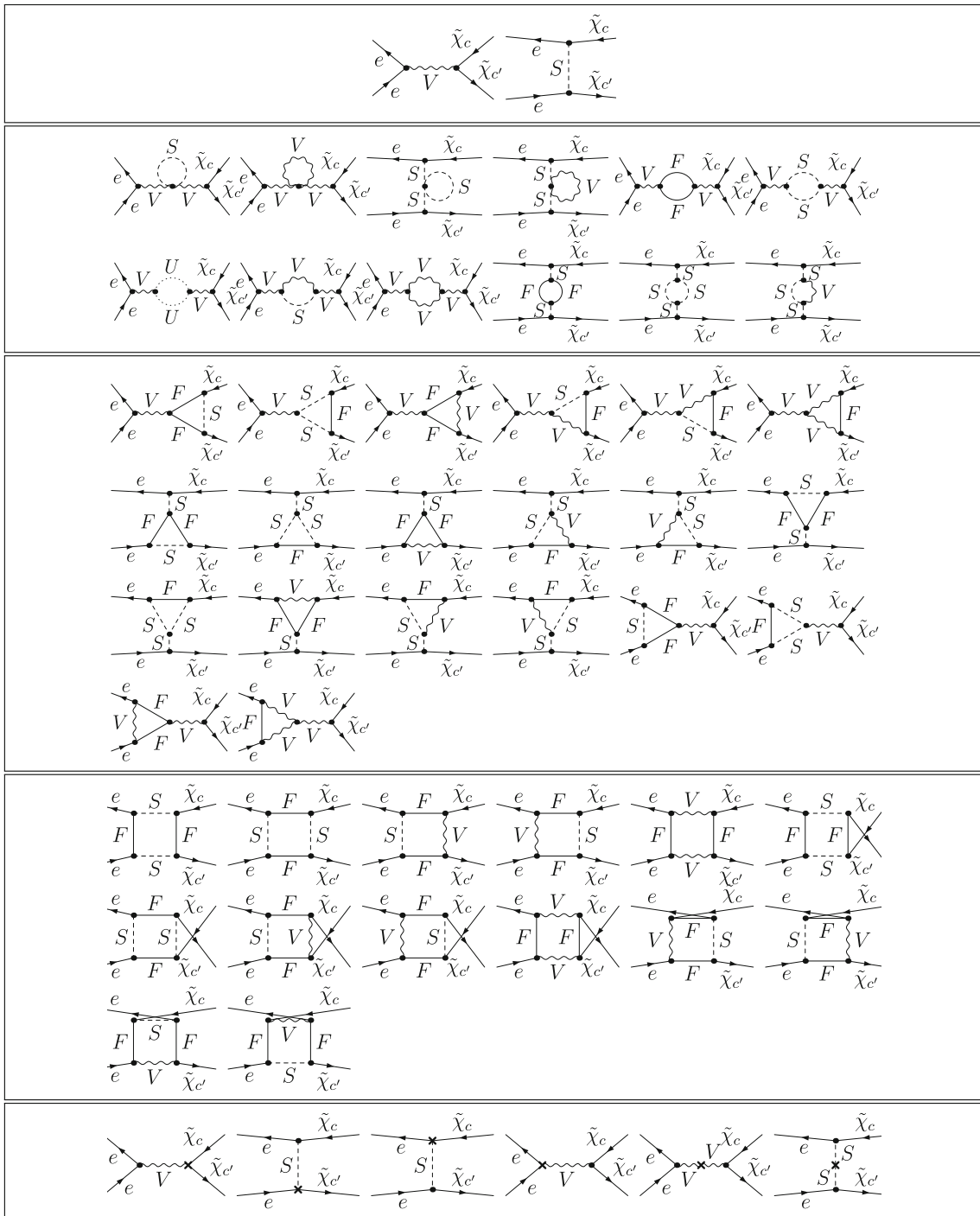


**Fig. 1** Generic tree, self-energy, vertex, box, and counterterm diagrams for the process  $e^+e^- \rightarrow \tilde{\chi}_c^\pm \tilde{\chi}_{c'}^\mp$  ( $c, c' = 1, 2$ ).  $F$  can be a SM fermion, chargino or neutralino;  $S$  can be a sfermion or

Higgs/Goldstone boson;  $V$  can be a  $\gamma$ ,  $Z$  or  $W^\pm$ . It should be noted that electron–Higgs couplings are neglected

ation. They are obtained from the corresponding tree-level diagrams by attaching a photon to the (incoming/outgoing) electron or chargino. The internal particles in the generically depicted diagrams in Figs. 1 and 2 are labeled as follows:  $F$  can be a SM fermion  $f$ , chargino  $\tilde{\chi}_c^\pm$  or neutralino

$\tilde{\chi}_n^0$ ;  $S$  can be a sfermion  $\tilde{f}_s$  or a Higgs (Goldstone) boson  $h^0, H^0, A^0, H^\pm$  ( $G, G^\pm$ );  $U$  denotes the ghosts  $u_V$ ;  $V$  can be a photon  $\gamma$  or a massive SM gauge boson,  $Z$  or  $W^\pm$ . We have neglected all electron–Higgs couplings and terms proportional to the electron mass whenever this is safe, i.e. except

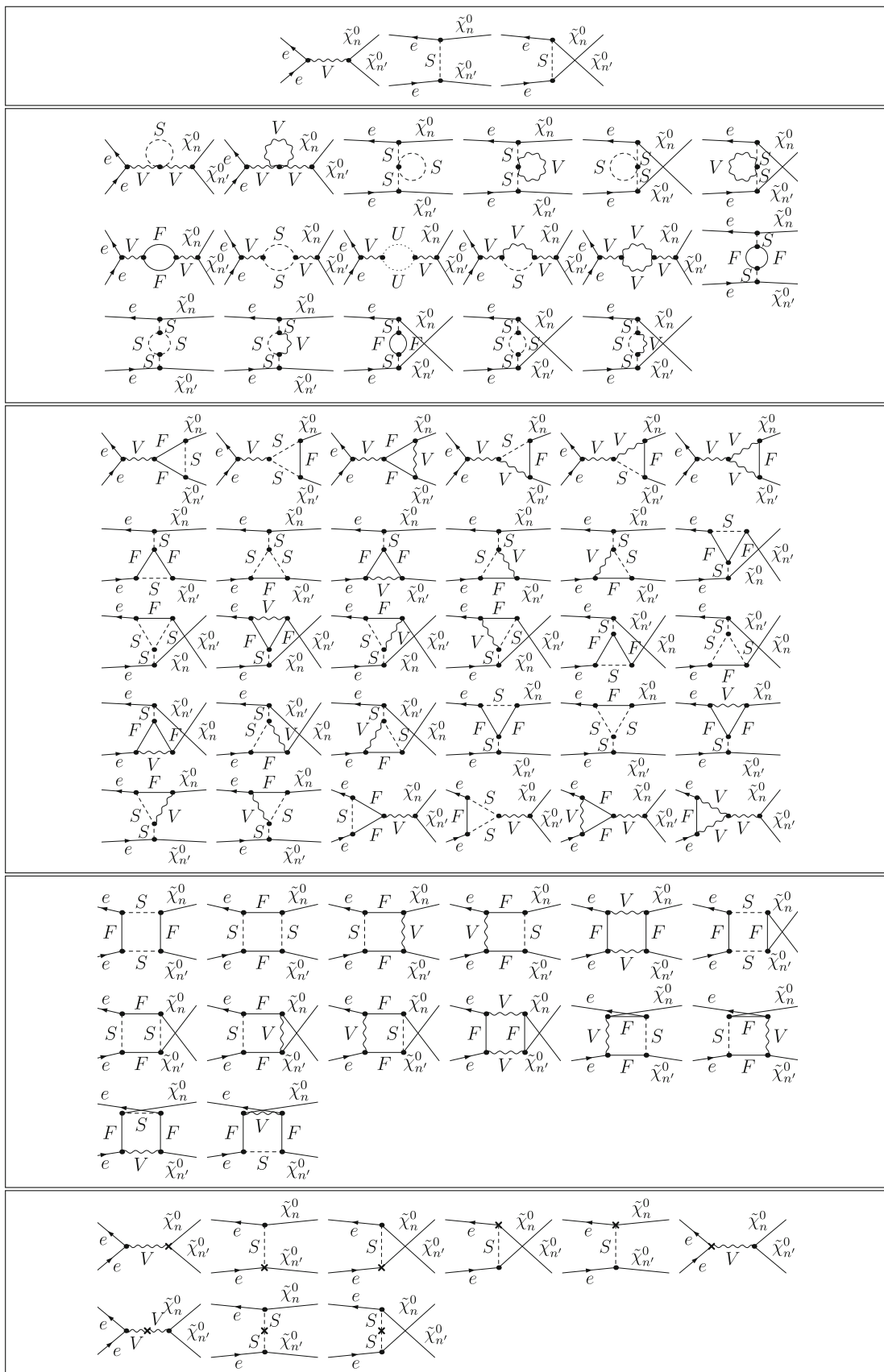


Fig. 2 Same as Fig. 1, but for the process  $e^+e^- \rightarrow \tilde{\chi}_n^0 \tilde{\chi}_{n'}^0$  ( $n, n' = 1, 2, 3, 4$ )

when the electron mass appears in negative powers or in loop integrals. We have verified numerically that these contributions are indeed totally negligible. For internally appearing Higgs bosons no higher-order corrections to their masses or couplings are taken into account; these corrections would correspond to effects beyond one-loop order.<sup>2</sup>

Moreover, in general, in Figs. 1 and 2 we have omitted diagrams with self-energy type corrections of external (on-shell) particles. While the contributions from the real parts of the loop functions are taken into account via the renormalization constants defined by OS renormalization conditions, the contributions coming from the imaginary part of the loop functions can result in an additional (real) correction if multiplied by complex parameters. In the analytical and numerical evaluation, these diagrams have been taken into account via the prescription described in Ref. [58].

Within our one-loop calculation we neglect finite width effects that can help to cure threshold singularities. Consequently, in the close vicinity of those thresholds our calculation does not give a reliable result. Switching to a complex mass scheme [73] would be another possibility to cure this problem, but its application is beyond the scope of our paper.

The tree-level formulas  $\sigma_{\text{tree}}(e^+e^- \rightarrow \tilde{\chi}_c^\pm \tilde{\chi}_{c'}^\mp)$  and  $\sigma_{\text{tree}}(e^+e^- \rightarrow \tilde{\chi}_n^0 \tilde{\chi}_{n'}^0)$  are rather lengthy and can be found elsewhere [30,31]. Concerning our evaluation of  $\sigma(e^+e^- \rightarrow \tilde{\chi}_c^\pm \tilde{\chi}_{c'}^\mp)$  we define

$$\begin{aligned} \sigma(e^+e^- \rightarrow \tilde{\chi}_c^\pm \tilde{\chi}_{c'}^\mp) &\equiv \sigma(e^+e^- \rightarrow \tilde{\chi}_c^+ \tilde{\chi}_{c'}^-) \\ &+ \sigma(e^+e^- \rightarrow \tilde{\chi}_c^- \tilde{\chi}_{c'}^+) \quad \forall c \neq c', \end{aligned} \quad (6)$$

if not indicated otherwise. Differences between the two charge conjugated processes can appear at the loop level when complex parameters are taken into account, as will be discussed in Sect. 4.2. We furthermore define the  $\mathcal{CP}$  asymmetry  $A_{12}$  for the non-diagonal chargino production (see Ref. [34] for details),

$$A_{12} := \frac{\sigma_{\text{full}}(e^+e^- \rightarrow \tilde{\chi}_1^+ \tilde{\chi}_2^-) - \sigma_{\text{full}}(e^+e^- \rightarrow \tilde{\chi}_1^- \tilde{\chi}_2^+)}{\sigma_{\text{tree}}(e^+e^- \rightarrow \tilde{\chi}_1^+ \tilde{\chi}_2^-) + \sigma_{\text{tree}}(e^+e^- \rightarrow \tilde{\chi}_1^- \tilde{\chi}_2^+)}. \quad (7)$$

This asymmetry will be used for a comparison with previous calculations and for an evaluation of the effects of the complex phases.

### 2.3 Ultraviolet, infrared and collinear divergences

As regularization scheme for the UV divergences we have used constrained differential renormalization [74], which has

<sup>2</sup> We found that using loop corrected Higgs-boson masses in the loops leads to a UV divergent result.

been shown to be equivalent to dimensional reduction [75,76] at the one-loop level [59,60]. Thus the employed regularization scheme preserves SUSY [77,78] and guarantees that the SUSY relations are kept intact, e.g., that the gauge couplings of the SM vertices and the Yukawa couplings of the corresponding SUSY vertices also coincide to one-loop order in the SUSY limit. Therefore no additional shifts, which might occur when using a different regularization scheme, arise. All UV divergences cancel in the final result.

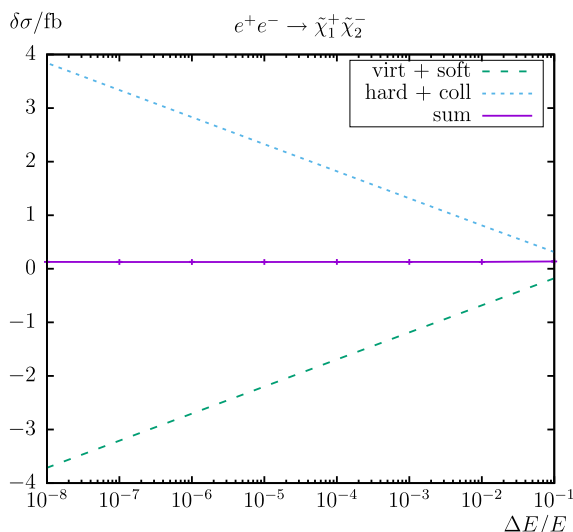
Soft photon emission implies numerical problems in the phase space integration of radiative processes. The phase space integral diverges in the soft energy region where the photon momentum becomes very small, leading to infrared (IR) singularities. Therefore the IR divergences from diagrams with an internal photon have to cancel with the ones from the corresponding real soft radiation. We have included the soft photon contribution via the code already implemented in `FormCalc` following the description given in Ref. [79]. The IR divergences arising from the diagrams involving a photon are regularized by introducing a photon mass parameter,  $\lambda$ . All IR divergences, i.e. all divergences in the limit  $\lambda \rightarrow 0$ , cancel once virtual and real diagrams for one process are added. We have numerically checked that our results do not depend on  $\lambda$  or on  $\Delta E = \delta_s E = \delta_s \sqrt{s}/2$  defining the energy cut that separates the soft from the hard radiation. As one can see from the example in Fig. 3 this holds for several orders of magnitude. Our numerical results below have been obtained for fixed  $\delta_s = 10^{-3}$ .

Numerical problems in the phase space integration of the radiative process arise also through collinear photon emission. Mass singularities emerge as a consequence of the collinear photon emission off massless particles. But already very light particles (such as electrons) can produce numerical instabilities. For the treatment of collinear singularities in the photon radiation off initial state electrons and positrons we used the phase space slicing method [80–83], which is not (yet) implemented in `FormCalc` and therefore we have developed and implemented the code necessary for the evaluation of collinear contributions; see also Refs. [67,68].

In the phase space slicing method, the phase space is divided into regions where the integrand is finite (numerically stable) and regions where it is divergent (or numerically unstable). In the stable regions the integration is performed numerically, whereas in the unstable regions it is carried out (semi-) analytically using approximations for the collinear photon emission.

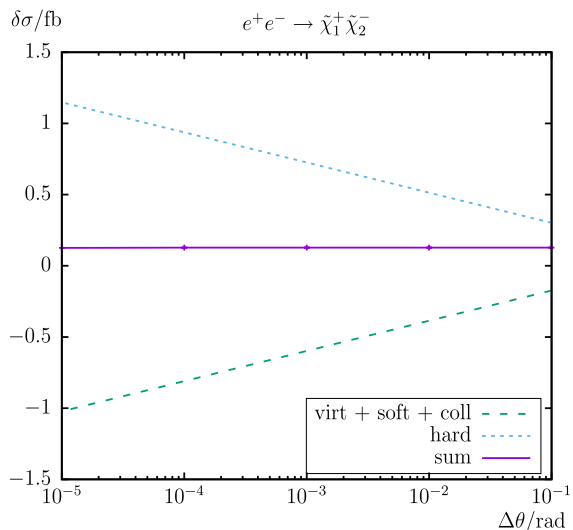
The collinear part is constrained by the angular cut-off parameter  $\Delta\theta$ , imposed on the angle between the photon and the (in our case initial state) electron/positron.

The differential cross section for the collinear photon radiation off the initial state  $e^+e^-$  pair corresponds to a convolution



$\Delta E/E$	$\delta\sigma/\text{fbarn}$
$10^{-1}$	$0.1366 \pm 0.0002$
$10^{-2}$	$0.1286 \pm 0.0005$
$10^{-3}$	$0.1277 \pm 0.0009$
$10^{-4}$	$0.1278 \pm 0.0012$
$10^{-5}$	$0.1274 \pm 0.0016$
$10^{-6}$	$0.1276 \pm 0.0018$
$10^{-7}$	$0.1271 \pm 0.0023$
$10^{-8}$	$0.1280 \pm 0.0026$

**Fig. 3** Phase space slicing method. The different contributions to the one-loop corrections  $\delta\sigma(e^+e^- \rightarrow \tilde{\chi}_1^\pm \tilde{\chi}_2^\mp)$  for our input parameter scenario  $S$  (see Table 2 below) as a function of  $\Delta E/E$  with fixed  $\Delta\theta/\text{rad} = 10^{-2}$



$\Delta\theta/\text{rad}$	$\delta\sigma/\text{fbarn}$
$10^0$	$0.1080 \pm 0.0012$
$10^{-1}$	$0.1276 \pm 0.0010$
$10^{-2}$	$0.1277 \pm 0.0009$
$10^{-3}$	$0.1277 \pm 0.0009$
$10^{-4}$	$0.1275 \pm 0.0010$
$10^{-5}$	$0.1259 \pm 0.0011$
$10^{-6}$	$0.0714 \pm 0.0013$

**Fig. 4** Phase space slicing method. The different contributions to the one-loop corrections  $\delta\sigma(e^+e^- \rightarrow \tilde{\chi}_1^\pm \tilde{\chi}_2^\mp)$  for our input parameter scenario  $S$  (see Table 2 below) as a function of  $\Delta\theta/\text{rad}$  with fixed  $\Delta E/E = 10^{-3}$

$$d\sigma_{\text{coll}}(s) = \frac{\alpha}{\pi} \int_0^{1-\delta_s} dz d\sigma_{\text{tree}}(\sqrt{zs}) \times \left\{ \left[ 2 \ln \left( \frac{\Delta\theta\sqrt{s}}{2m_e} \right) - 1 \right] P_{ee}(z) + 1 - z \right\}, \quad (8)$$

with  $P_{ee}(z) = (1 + z^2)/(1 - z)$  denoting the splitting function of a photon from the initial  $e^+e^-$  pair. The electron momentum is reduced (because of the radiated photon) by the fraction  $z$  such that the center-of-mass frame of the hard process receives a boost. The integration over all possible factors  $z$  is constrained by the soft cut-off  $\delta_s = \Delta E/E$ , to prevent over-counting in the soft energy region.

We have numerically checked that our results do not depend on the angular cut-off parameter  $\Delta\theta$  over several orders of magnitude; see the example in Fig. 4. Our numerical results below have been obtained for fixed  $\Delta\theta/\text{rad} = 10^{-2}$ .

The one-loop corrections of the differential cross section are decomposed into the virtual, soft, hard, and collinear parts as follows:

$$d\sigma_{\text{loop}} = d\sigma_{\text{virt}}(\lambda) + d\sigma_{\text{soft}}(\lambda, \Delta E) + d\sigma_{\text{hard}}(\Delta E, \Delta\theta) + d\sigma_{\text{coll}}(\Delta E, \Delta\theta). \quad (9)$$

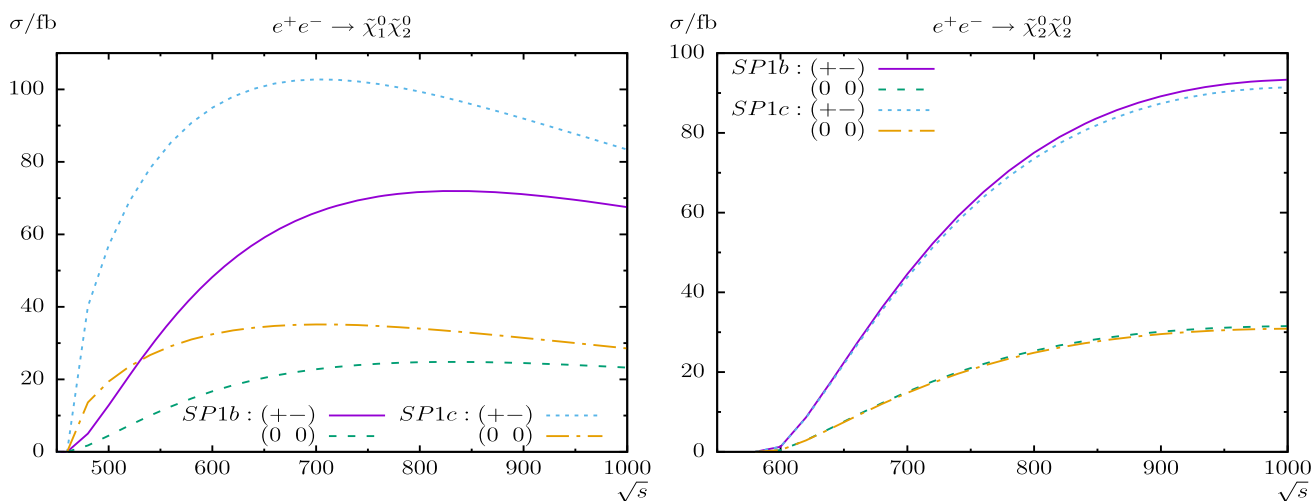


**Fig. 5** Comparison with Ref. [32] for  $\sigma(e^+e^- \rightarrow \tilde{\chi}_n^0 \tilde{\chi}_{n'}^0)$ . Tree cross sections are shown with parameters chosen according to Ref. [32] as a function of  $\sqrt{s}$ . The left (right) plot shows cross sections for

$e^+e^- \rightarrow \tilde{\chi}_1^0 \tilde{\chi}_2^0$  ( $e^+e^- \rightarrow \tilde{\chi}_2^0 \tilde{\chi}_2^0$ ). (+-) denotes (+0.60, -0.85) polarization of the positrons/electrons, whereas (0 0) denotes unpolarized positrons/electrons

The hard and collinear parts have been calculated via Monte Carlo integration algorithms of the CUBA library [84,85] as implemented in FormCalc [59,60].

### 3 Comparisons

In this section we present the comparisons with results from other groups in the literature for chargino/neutralino production in  $e^+e^-$  collisions. These comparisons were mostly restricted to the MSSM with real parameters. The level of agreement of such comparisons (at one-loop order) depends on the correct transformation of the input parameters from our renormalization scheme into the schemes used in the respective literature, as well as on the differences in the employed renormalization schemes as such. In view of the non-trivial conversions and the large number of comparisons such transformations and/or change of our renormalization prescription is beyond the scope of our paper.

- In Refs. [30,31] the processes  $e^+e^- \rightarrow \tilde{\chi}_c^\pm \tilde{\chi}_{c'}^\mp$  and  $e^+e^- \rightarrow \tilde{\chi}_n^0 \tilde{\chi}_{n'}^0$  have been calculated in the rMSSM at tree level. Because our tree-level results are in good agreement with other groups (see below), we omitted a comparison with Refs. [30,31].
- Tree-level results in the cMSSM for (polarized)  $e^+e^- \rightarrow \tilde{\chi}_n^0 \tilde{\chi}_{n'}^0$  (using a “projector formalism”) were presented in Ref. [32]. As input we used their parameter sets “SP1b” and “SP1c”, but it should be noted that they gave no SM input parameters. In Fig. 5 we show our calculation in comparison to their Fig. 6a, b where we find good agreement with their results. The small differences can be explained with the different SM input parameters.
- In Ref. [33] the process  $e^+e^- \rightarrow \tilde{\chi}_c^\pm \tilde{\chi}_{c'}^\mp$  ( $c \neq c'$ ) has been computed in the cMSSM (including “selected box contributions”) and extended to the full contributions in Refs. [34,35]. We performed a comparison with Ref. [34] using their input parameters (as far as possible). They also used (older versions of) FeynTools for their calculations. We find good agreement with their Fig. 3; as can be seen in our Fig. 6, where we show the  $\mathcal{CP}$ -odd observable  $A_{12}$ ; see Eq. (7). While the box contributions to  $A_{12}$  and the full results are in good agreement, the self-energy and vertex contributions differ significantly. However, here it should be noted that we have included the absorptive parts from self-energy type contributions via additional renormalization constants (see Refs. [58,64]) and not via the self-energy diagrams by themselves, which explains the large differences in the pure “self” and “vert” parts. But in combination the results are in agreement as expected. It should also be noted that  $A_{12}$  is very sensitive to the input parameters, explaining the small differences in the box and full results.
- Radiative corrections to chargino production in electron-positron collisions in the rMSSM were analyzed in Ref. [36]. The vertex corrections to  $e^+e^- \rightarrow \tilde{\chi}_c^\pm \tilde{\chi}_{c'}^\mp$  in the approximation of  $t/\tilde{t}/b/\tilde{b}$  contributions were evaluated, using an  $\overline{\text{MS}}$  renormalization scheme. It should be noted that Ref. [37] (see the next item) claimed differences to Ref. [36]. In addition this paper is (more or less) a prelude to Refs. [39,51], therefore we omitted a comparison with Ref. [36].
- In Ref. [37] the process  $e^+e^- \rightarrow \tilde{\chi}_c^\pm \tilde{\chi}_{c'}^\mp$  including all quark/squark contributions in the self-energy and vertex corrections has been calculated in the rMSSM. It should be noted that the authors claimed that the calculation of



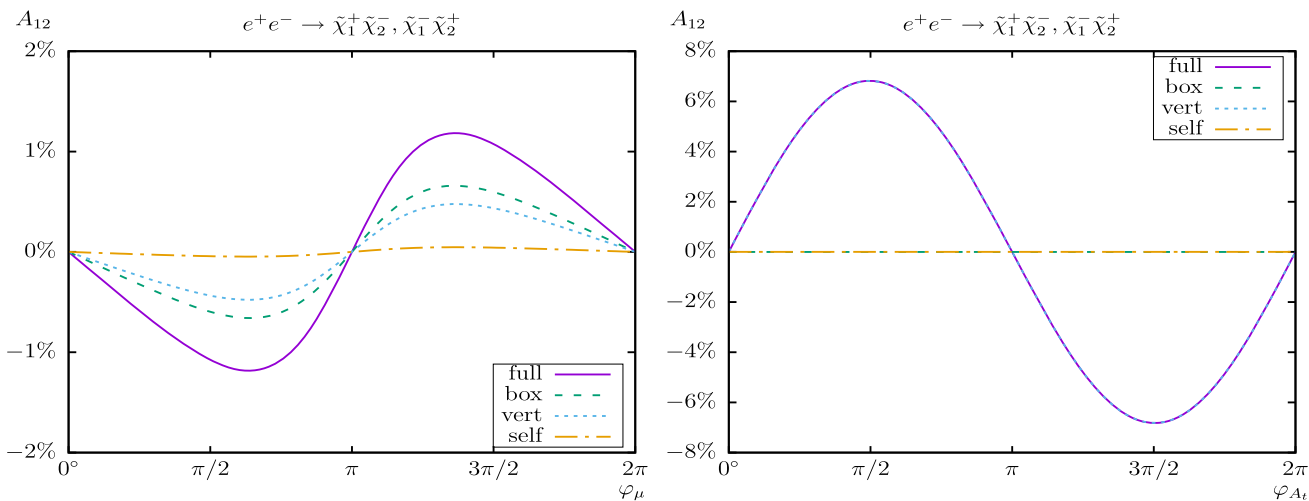


**Fig. 6** Comparison with Ref. [34] for  $\sigma(e^+e^- \rightarrow \tilde{\chi}_c^\pm \tilde{\chi}_c^\mp)$ .  $\mathcal{CP}$ -odd observables  $A_{12}$  are shown within scenario **a** chosen according to Ref. [34]. The left (right) plot shows  $A_{12}$  (see Eq. (7)) with  $\varphi_\mu$  ( $\varphi_{A_i}$ ) var-

ied and the different contributions from the box, vertex, and self-energy corrections including absorptive parts via renormalization constants

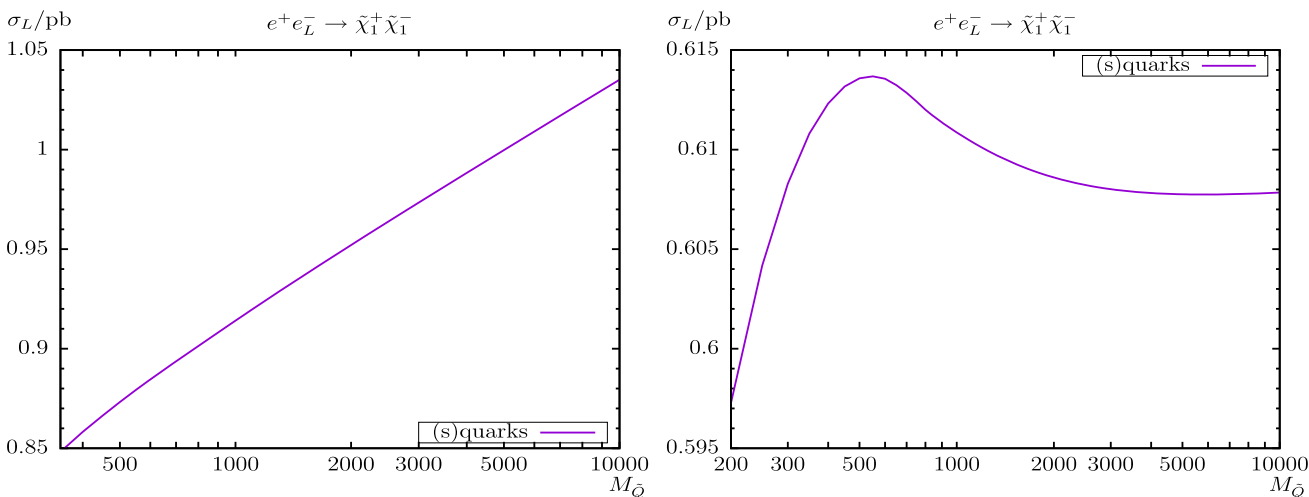


**Fig. 7** Comparison with Ref. [37] for  $\sigma(e^+e^-_L \rightarrow \tilde{\chi}_1^+ \tilde{\chi}_1^-)$ . The left (right) plot shows cross sections with  $M_{\tilde{Q}}$  varied for left-handed electrons and the parameter set G1 (H1) according to Ref. [37]

the cross section including only  $t/\tilde{t}/b/\tilde{b}$  loops as presented in Ref. [36] is not a reasonable approximation in general. We used their input parameters (i.e. scenarios G1 and H1) as far as possible (no SM parameters have been given)<sup>3</sup> and reproduced Figs. 1a and 3 of Ref. [37], where  $e^+e^-_L \rightarrow \tilde{\chi}_1^+ \tilde{\chi}_1^-$  had been evaluated. Our results are shown in Fig. 7. As in Ref. [37] we also include only the (s)quark contributions for this comparison. We have very good qualitative agreement and the loop corrections differ numerically less than 2%. The reasons for these small differences can again be found in the different renormalization schemes and SM input parameters.

- Full one-loop corrections in the rMSSM for  $e^+e^- \rightarrow \tilde{\chi}_c^\pm \tilde{\chi}_c^\mp$  were presented in Ref. [38]. Because Ref. [38] is only an extract from Ref. [44] (see the corresponding item below), we omitted a comparison with Ref. [38].
- In Ref. [39] the (weak) one-loop contributions of the rMSSM to the process  $e^+e^- \rightarrow \tilde{\chi}_c^\pm \tilde{\chi}_c^\mp$  have been calculated, i.e. neglecting the pure QED corrections involving photon loops and radiation. The calculation has been performed within the  $\overline{\text{DR}}$  scheme for polarized electrons and charginos. We used their input parameters (benchmark point C model) as far as possible and reproduced Figs. 3 and 4 of Ref. [39] in our Fig. 8. While we are in good qualitative agreement the loop corrections differ numerically. Besides the different renormalization schemes the

<sup>3</sup> As SM parameters we chose the PDG values from 1998.

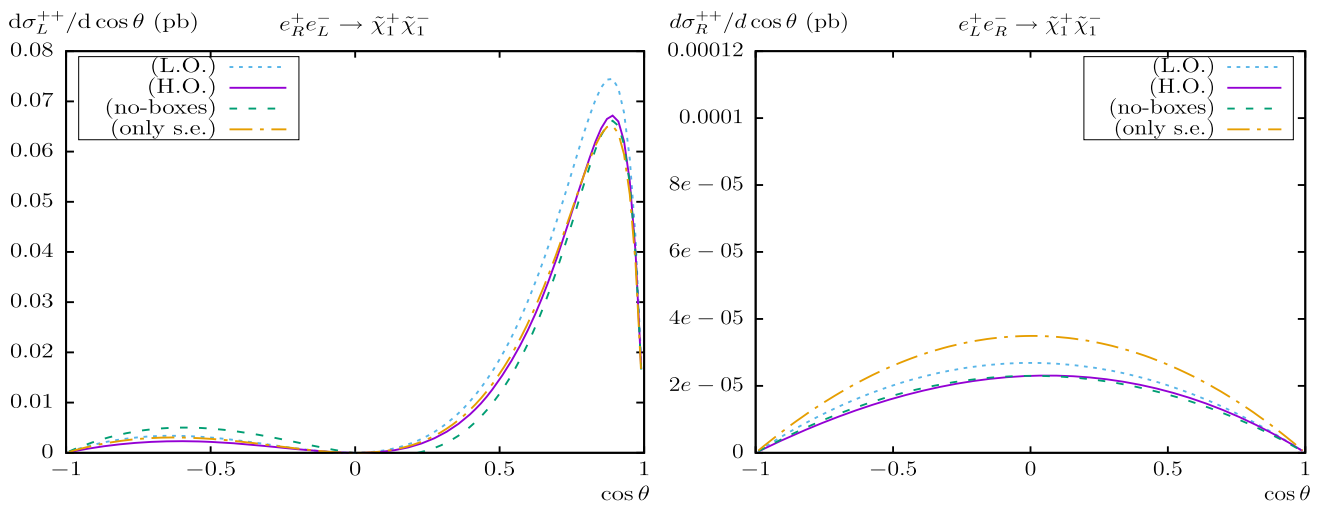


**Fig. 8** Comparison with Ref. [39] for  $\sigma(e^+e^- \rightarrow \tilde{\chi}_1^+ \tilde{\chi}_1^-)$ . The left (right) plot shows differential cross sections with  $\cos \theta$  varied for left-handed electrons, right-handed positrons (right-handed electrons, left-handed positrons) and charginos with positive helicity within the benchmark point C model according to Ref. [39]

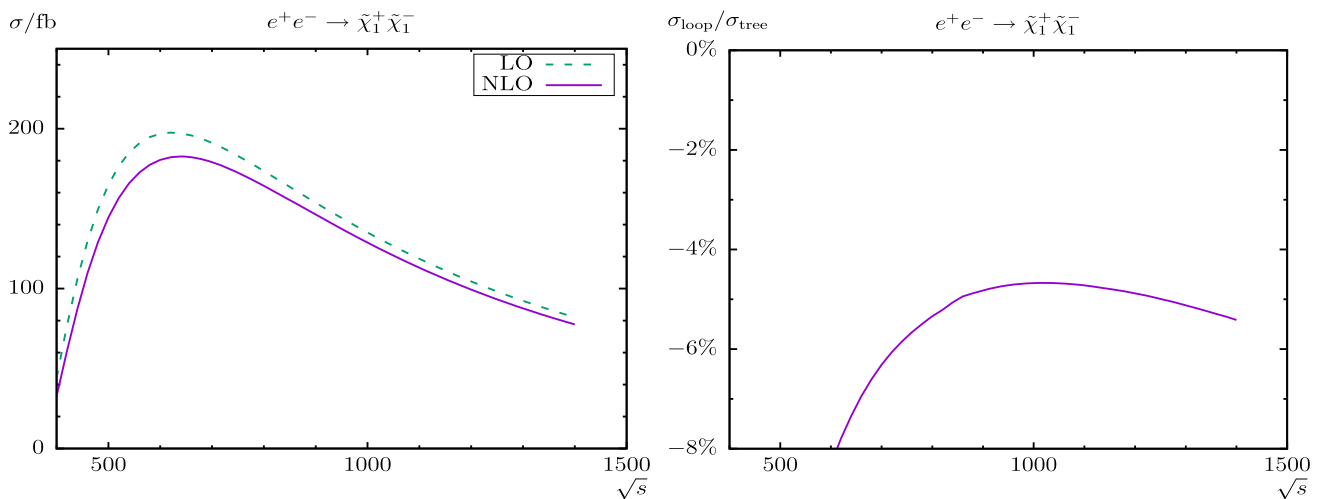


**Fig. 9** Comparison with Ref. [42] for  $\sigma(e^+e^- \rightarrow \tilde{\chi}_1^+ \tilde{\chi}_1^-)$ . The left (right) plot shows cross sections (relative corrections) with  $\sqrt{s}$  (in GeV) varied within the on-shell parameter set SPS1a'

main reason is that we must keep the QED corrections for UV finiteness in our on-shell scheme. Although we subtracted the leading QED logarithms  $\propto \ln(s/m_e^2)$  (by hand) for the comparison the differences are quite large, rendering this comparison not significant.

- The inclusion of multi-photon emission in  $e^+e^- \rightarrow \tilde{\chi}_c^\pm \tilde{\chi}_c^\mp$  and the implementation into an NLO event generator was presented in Refs. [42,43]. As input parameters they used the SUSY parameter point SPS1a'; see Ref. [86]. We also used the parameter point SPS1a' but translated from the  $\overline{\text{DR}}$  to on-shell values and reproduced successfully Fig. 7 of Ref. [42] in our Fig. 9. Our one-loop results are in reasonable agreement with the ones in Ref. [42] within  $\pm 3\%$ . The small difference

can easily be explained with the different renormalization schemes, slightly different input parameters, and the different treatment of the photon bremsstrahlung, where they have included multi-photon emission while we kept our calculation at  $\mathcal{O}(\alpha)$ .

- Ref. [44] is the source of Ref. [38] (see the corresponding previous item), dealing with chargino and neutralino production in the rMSSM. A comparison with Fig. 6.13 of Ref. [44] is given in our Fig. 10, where we show  $\tilde{\Delta} = (\sigma_{\text{loop}} - \sigma_{\text{ISR}})/\sigma_{\text{tree}}$  as a function of  $t_\beta$  for two numerical scenarios (used in the original Fig. 6.13).<sup>4</sup> Using their

<sup>4</sup> It should be noted that  $\sigma_{\text{ISR}}$  denotes the (large) initial state radiation  $\propto \ln(s/m_e^2)$ , whereas the hard and collinear photon radiation had been neglected in Ref. [44].

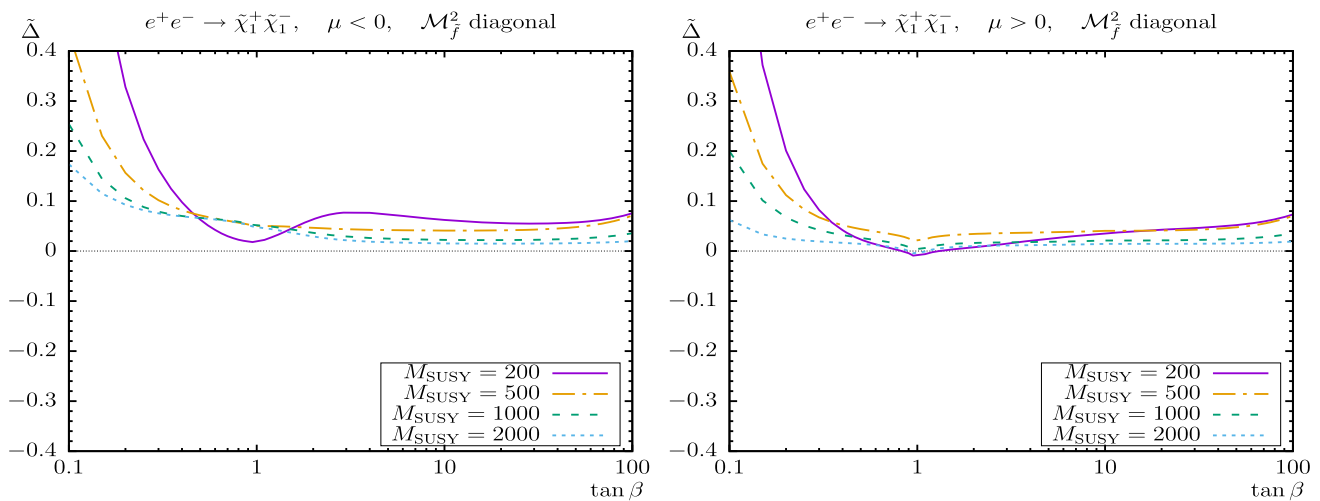


**Fig. 10** Comparison with Ref. [44] for  $\sigma(e^+e^- \rightarrow \tilde{\chi}_1^+ \tilde{\chi}_1^-)$ . The left (right) plot shows the relative corrections  $\tilde{\Delta}$  with  $t_\beta$  varied for  $\mu < 0$  ( $\mu > 0$ ) within the parameter set of Ref. [44]

input parameters and our CNN [2, 1, 3] scheme (which appears closest to their renormalization scheme) we are in rather good agreement for  $M_{\text{SUSY}} \geq 500$  GeV, while only in very rough agreement for  $M_{\text{SUSY}} = 200$  GeV. This can be explained with the different renormalization schemes, especially with the different renormalization of  $t_\beta$ , which in Ref. [44] is defined via the imaginary part of the AZ self-energy. Furthermore,  $\tilde{\Delta}$  is very sensitive to the loop corrections.

- Ref. [45] deals with “prototype graphs” for radiative corrections to polarized chargino or neutralino production in electron–positron annihilation. This paper contains no numerical analysis, rendering a comparison impossible.
- In Ref. [46] the “full” one-loop corrections to neutralino pair production in the rMSSM were analyzed numerically including QED corrections. They used (older versions of) `FeynTools` for their calculations but implemented their own on-shell renormalization procedure. In their analysis they show “full”  $\mathcal{O}(\alpha)$  corrections but without initial state radiation. The authors extended their analysis to  $e^+e^- \rightarrow \tilde{\chi}_n^0 \tilde{\chi}_{n'}^0$  and  $e^+e^- \rightarrow \tilde{\chi}_c^\pm \tilde{\chi}_{c'}^\mp$  in Ref. [47] in the cMSSM, making some improvements also concerning the photon radiation. Therefore, we skip the comparison with Ref. [46], but focus on Ref. [47]. We used their input parameters (i.e. the *real* on-shell parameter set of the SUSY parameter point SPS1a', see Ref. [86]) as far as possible and reproduced their Figs. 7, 8, 9, 10 and 11 in our Fig. 11. Qualitatively we are in good agreement with Ref. [47], but our (relative) one-loop results are numerically only roughly in agreement with their results within  $\pm 25\%$ . The differences can be explained (besides the different renormalization schemes) with the fact that they used an “ $\alpha(Q)$ ” scheme, which yields particularly large

corrections, w.r.t. our  $\alpha(0)$  scheme (these effects were known already for a long time; see Refs. [87–90], where the different renormalizations even yielded a different sign of the one-loop corrections). They also included higher-order contributions into their initial state radiation while we kept our calculation at  $\mathcal{O}(\alpha)$ .

- In Refs. [48–50] the processes  $e^+e^- \rightarrow \tilde{\chi}_c^\pm \tilde{\chi}_{c'}^\mp$  ( $c, c' = 1, 2$ ) and  $e^+e^- \rightarrow \tilde{\chi}_n^0 \tilde{\chi}_{n'}^0$  ( $n, n' = 1, 2, 3, 4$ ) have been calculated in the cMSSM, but only real parameters were included in the phenomenological analysis. Unfortunately, in Refs. [48, 49] not sufficient information as regards their input parameters were given, rendering a comparison impossible. On the other hand, both papers are contained in Ref. [50]. For the comparison with Ref. [50] we successfully reproduced their Table 7.1 (see our Table 1) and their Figs. 6.7, 7.2 and 7.3 (see our Fig. 12, where we show some examples). The (expected) *small* differences at  $\mathcal{O}(1\%)$  are likely caused by the slightly different renormalization scheme. An exception is  $e^+e^- \rightarrow \tilde{\chi}_3^0 \tilde{\chi}_3^0$ , where the tree-level cross section is accidentally very small, resulting in a larger deviation of the one-loop corrections.
- Finally, Ref. [51] is (more or less) an extension to Ref. [39] (see the corresponding previous item), dealing with polarized electrons and charginos and with multi-photon bremsstrahlung in the rMSSM. The authors claimed that they are in reasonable agreement with Ref. [47] within  $\pm 2\%$ . We used their input parameters as far as possible and reproduced their Fig. 6 in our Fig. 13. The relative corrections agree (away from the production threshold) better than  $\pm 10\%$ . The differences arise for the same reasons as already described in the comparison with Ref. [47]; see the corresponding item above.

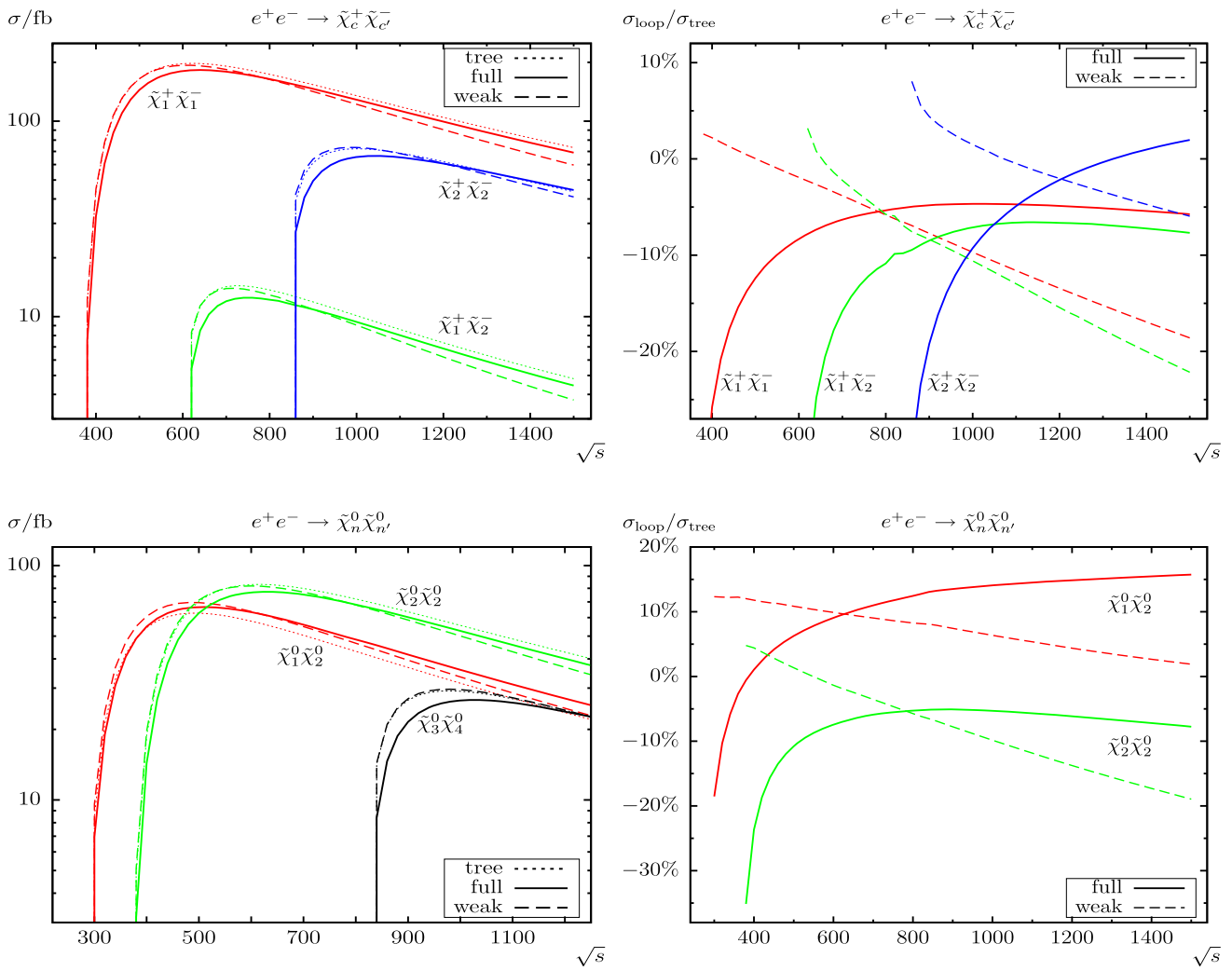


**Fig. 11** Comparison with Ref. [47] for  $\sigma(e^+e^- \rightarrow \tilde{\chi}_c^\pm \tilde{\chi}_{c'}^\mp)$  (upper row) and  $\sigma(e^+e^- \rightarrow \tilde{\chi}_n^0 \tilde{\chi}_{n'}^0)$  (lower row). The left (right) plot shows cross sections (relative corrections) with  $\sqrt{s}$  (in GeV) varied within the on-shell parameter set of SPS1a'

**Table 1** Comparison of the tree and one-loop corrected neutralino and chargino masses with Ref. [50] in the CCN[1] scheme. All masses are in GeV

	$m_{\tilde{\chi}_1^0}$	$m_{\tilde{\chi}_2^0}$	$m_{\tilde{\chi}_3^0}$	$m_{\tilde{\chi}_4^0}$	$m_{\tilde{\chi}_1^\pm}$	$m_{\tilde{\chi}_2^\pm}$
Tree						
Ref. [50]	97.75	184.55	405.10	420.46	184.20	421.24
FeynTools	97.75	184.55	405.09	420.46	184.20	421.24
Loop						
Ref. [50]	97.75	184.44	407.46	419.45	184.20	421.24
FeynTools	97.75	184.43	407.44	419.45	184.20	421.24

- The effects of imaginary and absorptive parts were analyzed for  $e^+e^- \rightarrow \tilde{\chi}_c^\pm \tilde{\chi}_{c'}^\mp$  in Ref. [52]. The differences in the renormalization of the chargino/neutralino sector between Ref. [52] and our work are discussed in Ref. [27]. The chargino/neutralino production in the cMSSM at the full one-loop level has been numerically compared with Ref. [52] using their latest FeynArts model file implementation. We found overall agreement better than 4%

(in most cases better than 1%) in the loop corrections for real and complex parameters.<sup>5</sup>

- For the precise extraction of the underlying SUSY parameters, in Ref. [53]  $e^+e^- \rightarrow \tilde{\chi}_c^\pm \tilde{\chi}_{c'}^\mp$  has been calcu-

<sup>5</sup> It should be noted that the original code used for Ref. [52] is no longer available [91], where we found significant numerical differences with the results shown in Ref. [52].

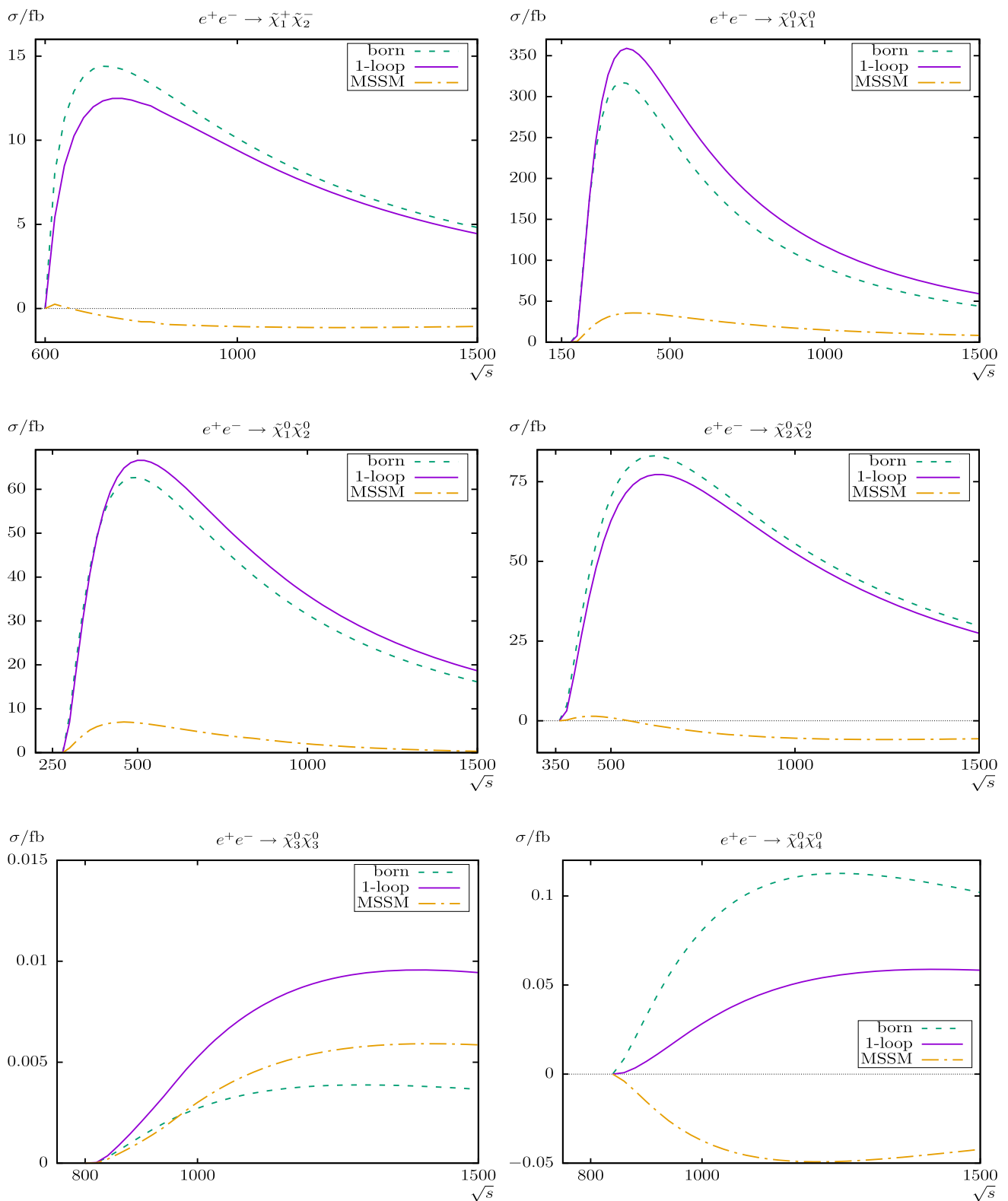


**Fig. 12** Comparison with Ref. [50] for  $\sigma(e^+e^- \rightarrow \tilde{\chi}_c^\pm \tilde{\chi}_{c'}^\mp)$  and  $\sigma(e^+e^- \rightarrow \tilde{\chi}_n^0 \tilde{\chi}_{n'}^0)$ . As example some of the cross sections (in fb) are shown with the on-shell parameter set SPS1a' chosen according to Ref. [50], varied with  $\sqrt{s}$  (in GeV)

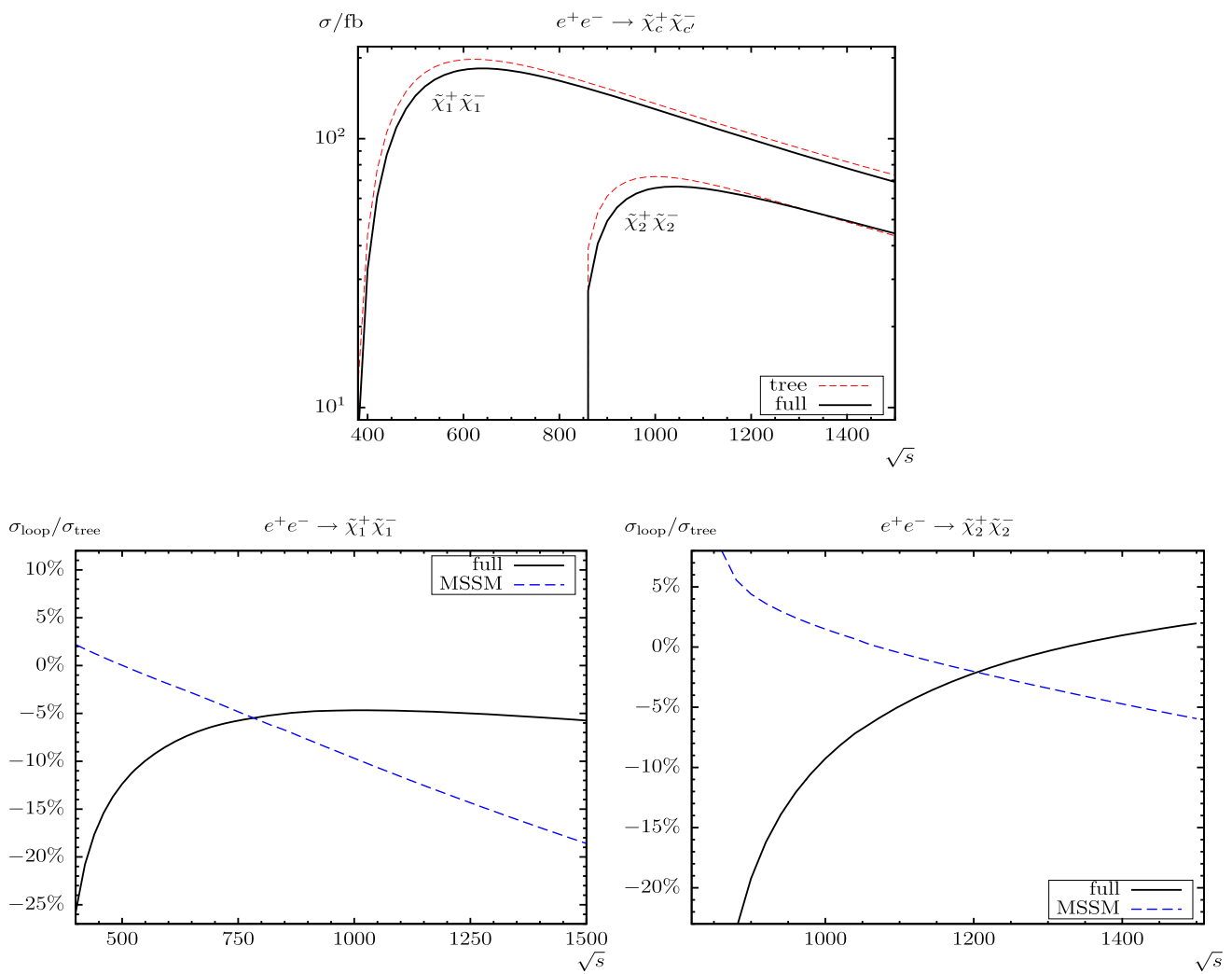


**Fig. 13** Comparison with Ref. [51] for  $\sigma(e^+e^- \rightarrow \tilde{\chi}_c^\pm \tilde{\chi}_c^\mp)$ . The upper (lower) plot(s) shows cross sections (relative corrections) with  $\sqrt{s}$  (in GeV) varied within the SUSY parameter point SPS1a'

lated at the full one-loop level for three cMSSM benchmark points. As in the previous point, the differences in the renormalization of the chargino/neutralino sector between Ref. [53] and our work are discussed in Ref. [27]. Again, using their latest FeynArts model file implementation, we found overall agreement better than 2% in the loop corrections. But we found significant numerical differences with the results shown in Ref. [53], as already noted in the previous item.

To conclude, we found good agreement with the literature where expected, and the encountered differences can be traced back to different renormalization schemes, corresponding mismatches in the input parameters and small differences in the SM parameters. After comparing with the existing literature we would like to stress again that here we present for the first time a full one-loop calculation of  $\sigma(e^+e^- \rightarrow \tilde{\chi}_n^0 \tilde{\chi}_{n'}^0)$  and  $\sigma(e^+e^- \rightarrow \tilde{\chi}_c^\pm \tilde{\chi}_{c'}^\mp)$  in the cMSSM,

using the scheme that was employed successfully already for the full one-loop decays of the (produced) charginos and neutralinos. The two calculations can readily be used together for the full production and decay chain.

#### 4 Numerical analysis

In this section we present our numerical analysis of chargino/neutralino production at  $e^+e^-$  colliders in the cMSSM. In the figures below we show the cross sections at the tree level (“tree”) and at the full one-loop level (“full”), which is the cross section including *all* one-loop corrections as described in Sect. 2. The CCN[1] scheme (i.e. OS conditions for the two charginos and the lightest neutralino) has been used for most evaluations. For comparative calculations also some CNN[ $c, n, n'$ ] schemes (OS conditions for one chargino and two neutralinos) have been used, as indicated below.

**Table 2** MSSM default parameters for the numerical investigation; all parameters (except of  $t_\beta$ ) are in GeV. The values for the trilinear sfermion Higgs couplings,  $A_{t,b,\tau}$  are chosen to be real and such that charge- and/or color-breaking minima are avoided [96–102]. (It should be noted that we chose common values for the three sfermion genera-

tions.) For the charginos and neutralinos we show the tree-level values as well as their OS masses in the CCN [1], CNN [1, 1, 3], CNN [1, 1, 4], CNN [2, 1, 2], and CNN [2, 1, 3] scheme as obtained from Eq. (5). Also shown are some values for the complex phase  $\varphi_{M_1}$  in the CCN [1] scheme

Scen.	$\sqrt{s}$	$t_\beta$	$\mu$	$M_{H^\pm}$	$M_{\tilde{Q},\tilde{U},\tilde{D}}$	$M_{\tilde{L},\tilde{E}}$	$ A_t $	$A_b$	$A_\tau$	$ M_1 $	$M_2$	$M_3$
$\mathcal{S}$	1000	10	450	500	1500	1500	2000	$ A_t $	$M_{\tilde{L}}$	$\mu/4$	$\mu/2$	2000
			$m_{\tilde{\chi}_1^\pm}$	$m_{\tilde{\chi}_2^\pm}$	$m_{\tilde{\chi}_1^0}$	$m_{\tilde{\chi}_2^0}$	$m_{\tilde{\chi}_3^0}$	$m_{\tilde{\chi}_4^0}$				
tree			212.760	469.874	110.434	213.002	455.162	469.226				
CCN [1]			212.760	469.874	110.434	212.850	455.195	469.560				
$\varphi_{M_1} = 90^\circ$			212.760	469.874	111.356	212.722	455.628	468.972				
$\varphi_{M_1} = 180^\circ$			212.760	469.874	112.274	212.593	456.105	468.340				
CNN [1, 1, 3]			212.760	469.844	110.434	212.850	455.162	469.530				
CNN [1, 1, 4]			212.760	469.539	110.434	212.850	454.837	469.226				
CNN [2, 1, 2]			212.912	469.874	110.434	213.002	455.184	469.561				
CNN [2, 1, 3]			213.214	469.874	110.434	213.303	455.162	469.563				

We first define the numerical scenario for the cross section evaluation. Then we start the numerical analysis with the cross sections of  $e^+e^- \rightarrow \tilde{\chi}_c^\pm \tilde{\chi}_{c'}^\mp$  ( $c, c' = 1, 2$ ) in Sect. 4.2, evaluated as a function of  $\sqrt{s}$  (up to 3 TeV, shown in the upper left plot of the respective figures),  $\mu$  (starting at  $\mu = 240$  GeV up to  $\mu = 2000$  GeV, shown in the upper right plots),  $M_{\tilde{L},\tilde{E}}$  (from 200 to 2000 GeV, lower left or middle plots)<sup>6</sup> and  $\varphi_{M_1}$  (between  $0^\circ$  and  $360^\circ$ , lower right or middle plots). In some cases also the  $t_\beta$  dependence is shown. Then we turn to the processes  $e^+e^- \rightarrow \tilde{\chi}_n^0 \tilde{\chi}_{n'}^0$  ( $n, n' = 1, 2, 3, 4$ ) in Sect. 4.3. All these processes are of particular interest for ILC (with  $\sqrt{s} \lesssim 1$  TeV) and CLIC (with  $\sqrt{s} \lesssim 3$  TeV) analyses [14–18, 20, 21] (as emphasized in Sect. 1).

### 4.1 Parameter settings

The renormalization scale  $\mu_R$  has been set to the center-of-mass energy,  $\sqrt{s}$ . The SM parameters are chosen as follows; see also [95]:

- Fermion masses (on-shell masses, if not indicated differently):

$$\begin{aligned}
 m_e &= 0.5109989461 \text{ MeV}, & m_{\nu_e} &= 0, \\
 m_\mu &= 105.6583745 \text{ MeV}, & m_{\nu_\mu} &= 0, \\
 m_\tau &= 1776.86 \text{ MeV}, & m_{\nu_\tau} &= 0, \\
 m_u &= 71.03 \text{ MeV}, & m_d &= 71.03 \text{ MeV},
 \end{aligned}$$

<sup>6</sup> It should be noted that the lowest resulting selectron or slepton masses can have an impact on the search limits for the charginos/neutralinos [92–94]. However, a detailed analysis of the excluded parameter space is outside of the scope of our numerical evaluation.

$$\begin{aligned}
 m_c &= 1.27 \text{ GeV}, & m_s &= 96.0 \text{ MeV}, \\
 m_t &= 173.21 \text{ GeV}, & m_b &= 4.66 \text{ GeV}.
 \end{aligned}
 \tag{10}$$

According to Ref. [95],  $m_s$  is an estimate of a so-called “current quark mass” in the  $\overline{\text{MS}}$  scheme at the scale  $\mu \approx 2$  GeV.  $m_c \equiv m_c(m_c)$  is the “running” mass in the  $\overline{\text{MS}}$  scheme and  $m_b$  is the  $\Upsilon(1S)$  bottom quark mass.  $m_u$  and  $m_d$  are effective parameters, calculated through the hadronic contributions to

$$\begin{aligned}
 \Delta\alpha_{\text{had}}^{(5)}(M_Z) &= \frac{\alpha}{\pi} \sum_{f=u,c,d,s,b} Q_f^2 \left( \ln \frac{M_Z^2}{m_f^2} - \frac{5}{3} \right) \\
 &\approx 0.02764.
 \end{aligned}
 \tag{11}$$

- Gauge-boson masses:

$$M_Z = 91.1876 \text{ GeV}, \quad M_W = 80.385 \text{ GeV}.
 \tag{12}$$

- Coupling constant:

$$\alpha(0) = 1/137.035999139.
 \tag{13}$$

The SUSY parameters are chosen according to the scenario  $\mathcal{S}$ , shown in Table 2.<sup>7</sup> This scenario is viable for the various cMSSM chargino/neutralino production modes, i.e. not picking specific parameters for each cross section. They are in particular in agreement with the chargino and neutralino searches of ATLAS [92] and CMS [93, 94]. Here it should be noted that a small increase in  $\mu$  by 20%, the decay channel  $\tilde{\chi}_2^0 \rightarrow \tilde{\chi}_1^0 h$  opens up, and the excluded parameter space

<sup>7</sup> It should be noted that changing  $\mu$  also (by default) changes  $M_1$  and  $M_2$  in our scenario  $\mathcal{S}$ .

shrinks significantly [92–94]. The masses are chosen such that for the default benchmark *all* chargino/neutralino production modes are accessible at the ILC (and thus at CLIC).

It should be noted that higher-order corrected Higgs-boson masses do not enter our calculation.<sup>8</sup> However, we ensured that over larger parts of the parameter space the lightest Higgs-boson mass is around  $\sim 125 \pm 3$  GeV to indicate the phenomenological validity of our scenarios. In our numerical evaluation we will show the variation with  $\sqrt{s}$ ,  $\mu$ ,  $M_{\tilde{L}} = M_{\tilde{E}}$ , and  $\varphi_{M_1}$ , the phase of  $M_1$ . The dependence of  $t_\beta$  turned out to be rather small, therefore we show it only in a few cases, where it is of special interest.

Concerning the complex parameters, some more comments are in order. Potentially complex parameters that enter the chargino/neutralino production cross sections at tree level are the soft SUSY-breaking parameters  $M_1$  and  $M_2$  as well as the Higgs mixing parameter  $\mu$ . However, when performing an analysis involving complex parameters it should be noted that the results for physical observables are affected only by certain combinations of the complex phases of the parameters  $\mu$ , the trilinear couplings  $A_f$  and the gaugino mass parameters  $M_{1,2,3}$  [104, 105]. It is possible, for instance, to rotate the phase  $\varphi_{M_2}$  away. Experimental constraints on the (combinations of) complex phases arise, in particular, from their contributions to electric dipole moments of the electron and the neutron (see Refs. [106–108] and the references therein), of the deuteron [109] and of heavy quarks [110, 111]. While SM contributions enter only at the three-loop level, due to its complex phases the MSSM can contribute already at one-loop order. Large phases in the first two generations of sfermions can only be accommodated if these generations are assumed to be very heavy [112, 113] or large cancellations occur [114–116]; see, however, the discussion in Ref. [117]. A review can be found in Ref. [118]. Recently additional constraints at the two-loop level on some  $\mathcal{CP}$  phases of SUSY models have been investigated in Ref. [119]. Accordingly (using the convention that  $\varphi_{M_2} = 0$ , as done in this paper), in particular, the phase  $\varphi_\mu$  is tightly constrained [120], and we set it to zero. On the other hand, the bounds on the phases of the third-generation trilinear couplings are much weaker. Consequently, the largest effects on the neutralino production cross sections at the tree level are expected from the complex gaugino mass parameter  $M_1$ , i.e. from  $\varphi_{M_1}$ . At the loop level the largest effects are expected from contributions involving large Yukawa couplings, and thus  $\varphi_{A_t}$  potentially has the strongest impact. This motivates our choice of  $\varphi_{M_1}$  and  $\varphi_{A_t}$  as parameters to be varied.

<sup>8</sup> Since we work in the MSSM with complex parameters,  $M_{H^\pm}$  is chosen as input parameter, and higher-order corrections affect only the neutral Higgs-boson spectrum; see Ref. [103] for the most recent evaluation.

Since now complex parameters can appear in the couplings, contributions from absorptive parts of self-energy type corrections on external legs can arise. The corresponding formulas for an inclusion of these absorptive contributions via finite wave function correction factors can be found in Refs. [58, 64].

The numerical results shown in the next subsections are of course dependent on the choice of the SUSY parameters. Nevertheless, they give an idea of the relevance of the full one-loop corrections.

#### 4.2 The process $e^+e^- \rightarrow \tilde{\chi}_c^\pm \tilde{\chi}_{c'}^\mp$

The process  $e^+e^- \rightarrow \tilde{\chi}_1^+ \tilde{\chi}_1^-$  is shown in Fig. 14. It should be noted that for  $s \rightarrow \infty$  decreasing cross sections  $\propto 1/s$  are expected; see Ref. [30]. If not indicated otherwise, unpolarized electrons and positrons are assumed. We also remind the reader that  $\sigma(e^+e^- \rightarrow \tilde{\chi}_c^\pm \tilde{\chi}_{c'}^\mp)$  denotes the sum of the two charge conjugated processes  $\forall c \neq c'$ ; see Eq. (6).

In the analysis of the production cross section as a function of  $\sqrt{s}$  (upper left plot) we find the expected behavior: a strong rise close to the production threshold, followed by a decrease with increasing  $\sqrt{s}$ . We find a very small shift w.r.t.  $\sqrt{s}$  around the production threshold (not visible in the plot). Away from the production threshold, loop corrections of  $\sim -8\%$  at  $\sqrt{s} = 500$  GeV and  $\sim +14\%$  at  $\sqrt{s} = 1000$  GeV are found in scenario  $\mathcal{S}$  (see Table 2), with a “tree crossing” (i.e. where the loop corrections become approximately zero and therefore cross the tree-level result) at  $\sqrt{s} \approx 575$  GeV. The relative size of loop corrections increase with increasing  $\sqrt{s}$  (and decreasing  $\sigma$ ) and reach  $\sim +19\%$  at  $\sqrt{s} = 3000$  GeV.

With increasing  $\mu$  in  $\mathcal{S}$  (upper right plot) we find a strong decrease of the production cross section, as can be expected from kinematics, discussed above. The relative loop corrections in  $\mathcal{S}$  reach  $\sim +30\%$  at  $\mu = 240$  GeV (at the border of the experimental limit),  $\sim +14\%$  at  $\mu = 450$  GeV (i.e.  $\mathcal{S}$ ) and  $\sim -30\%$  at  $\mu = 1000$  GeV. In the latter case these large loop corrections are due to the (relative) smallness of the tree-level results, which goes to zero for  $\mu = 1020$  GeV (i.e. the chargino production threshold).

The cross section as a function of  $M_{\tilde{L}} (= M_{\tilde{E}})$  is shown in the lower left plot of Fig. 14. This mass parameter controls the  $t$ -channel exchange of first generation sleptons at tree level. First a small decrease down to  $\sim 90$  fb can be observed for  $M_{\tilde{L}} \approx 400$  GeV. For larger  $M_{\tilde{L}}$  the cross section rises up to  $\sim 190$  fb for  $M_{\tilde{L}} = 2$  TeV. In scenario  $\mathcal{S}$  we find a substantial increase of the cross sections from the loop corrections. They reach the maximum of  $\sim +18\%$  at  $M_{\tilde{L}} \approx 850$  GeV with a nearly constant offset of about 20 fb for higher values of  $M_{\tilde{L}}$ .

Due to the absence of  $\varphi_{M_1}$  in the tree-level production cross section the effect of this complex phase is expected to be small. Correspondingly we find that the phase dependence



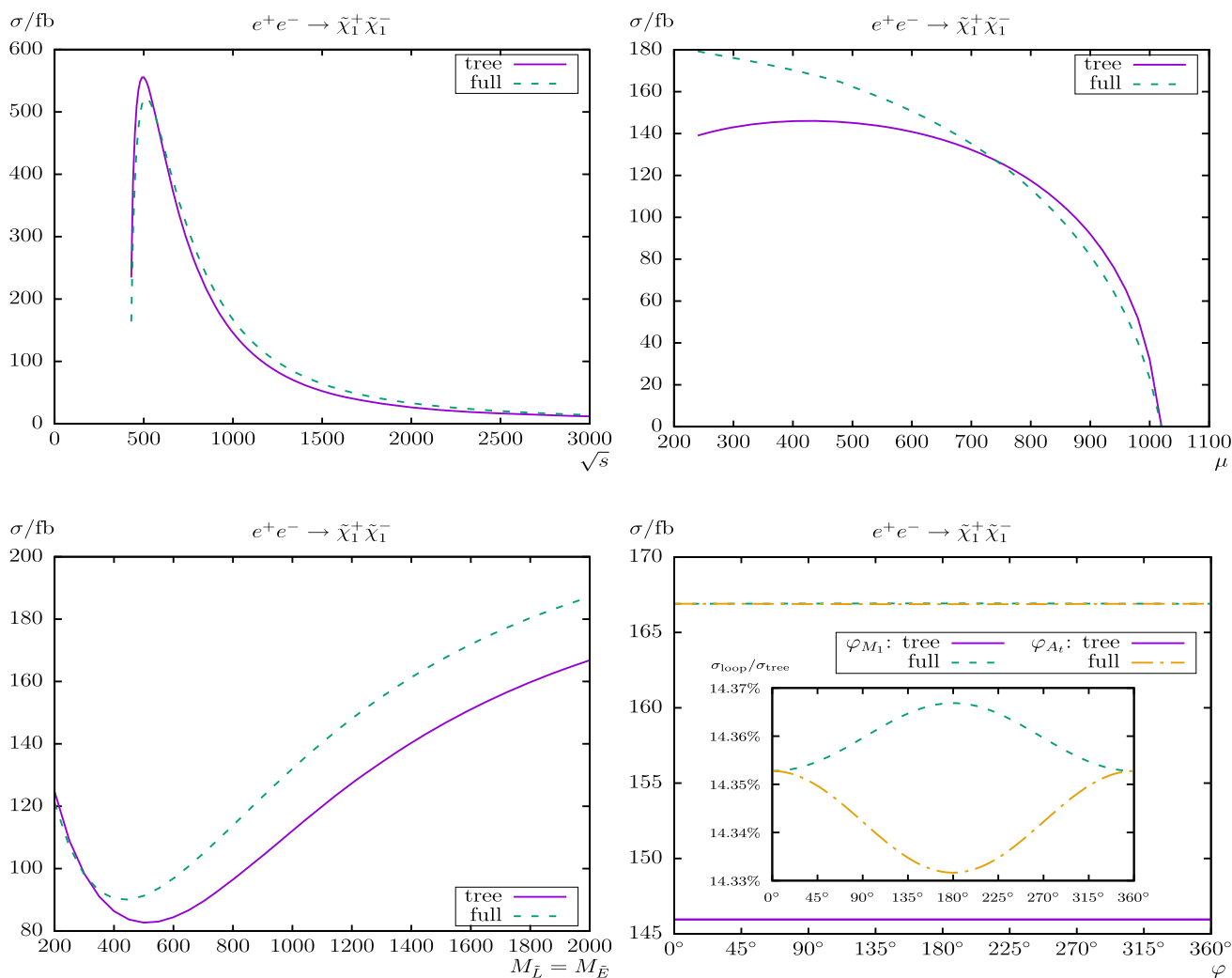


**Fig. 14**  $\sigma(e^+e^- \rightarrow \tilde{\chi}_1^+ \tilde{\chi}_1^-)$ . Tree-level and full one-loop corrected cross sections are shown with parameters chosen according to  $\mathcal{S}$ ; see Table 2. The upper plots show the cross sections with  $\sqrt{s}$  (left) and  $\mu$  (right) varied; the lower plots show  $M_{\tilde{L}} = M_{\tilde{E}}$  (left) and  $\varphi_{M_1}, \varphi_{A_t}$  (right) varied

$\varphi_{M_1}$  of the cross section in our scenario is tiny. The loop corrections are found to be nearly independent of  $\varphi_{M_1}$  at the level below  $\sim +0.1\%$  in  $\mathcal{S}$ . We also show the variation with  $\varphi_{A_t}$ , which enter via final state vertex corrections. While the variation with  $\varphi_{A_t}$  is somewhat larger than with  $\varphi_{M_1}$ , it remains tiny and unobservable.

In Fig. 15 we present the cross sections  $e^+e^- \rightarrow \tilde{\chi}_1^\pm \tilde{\chi}_2^\mp$ . In the analysis as a function of  $\sqrt{s}$  (upper left plot) we find as before a tiny shift w.r.t.  $\sqrt{s}$ , where the position of the maximum cross section shifts by about +50 GeV. The relative corrections are found to be of  $\sim +8\%$  at  $\sqrt{s} = 1000$  GeV (i.e.  $\mathcal{S}$ ), and  $\sim -20\%$  at  $\sqrt{s} = 3000$  GeV. The peak (hardly visible in the dotted line) at  $\sqrt{s} \approx 940$  GeV is the production threshold  $m_{\tilde{\chi}_2^\pm} + m_{\tilde{\chi}_1^\pm} = \sqrt{s}$ .

The dependence on  $\mu$  (upper row, right plot) is nearly linear, and mostly due to kinematics. The loop corrections

are  $\sim +17\%$  at  $\mu = 240$  GeV,  $\sim +8\%$  at  $\mu = 450$  GeV (i.e.  $\mathcal{S}$ ), and  $\sim -27\%$  at  $\mu = 660$  GeV where the tree level goes to zero (i.e. the chargino production threshold). These large loop corrections are again due to the (relative) smallness of the tree-level results at  $\mu \approx 660$  GeV.

As a function of  $M_{\tilde{L}}$  (middle left plot) the cross section is rather flat for  $M_{\tilde{L}} \gtrsim 800$  GeV. The relative corrections increase from  $\sim -16\%$  at  $\mu = 400$  GeV to  $\sim +8\%$  at  $\mu = 1300$  GeV, with a tree crossing at  $\mu \approx 800$  GeV.

The dependence on  $\varphi_{M_1}$  (middle right plot) is again very small, the loop corrections are found to be nearly independent of  $\varphi_{M_1}$  below the level of  $\sim +0.1\%$ . We show separately the cross sections for  $e^+e^- \rightarrow \tilde{\chi}_1^+ \tilde{\chi}_2^-$  and  $e^+e^- \rightarrow \tilde{\chi}_1^- \tilde{\chi}_2^+$ . As the inlay shows, they differ from each other, but only at an (experimentally indistinguishable) level of  $\mathcal{O}(0.1\%)$ . In addition we also show here the dependence on  $\varphi_{A_t}$ , which

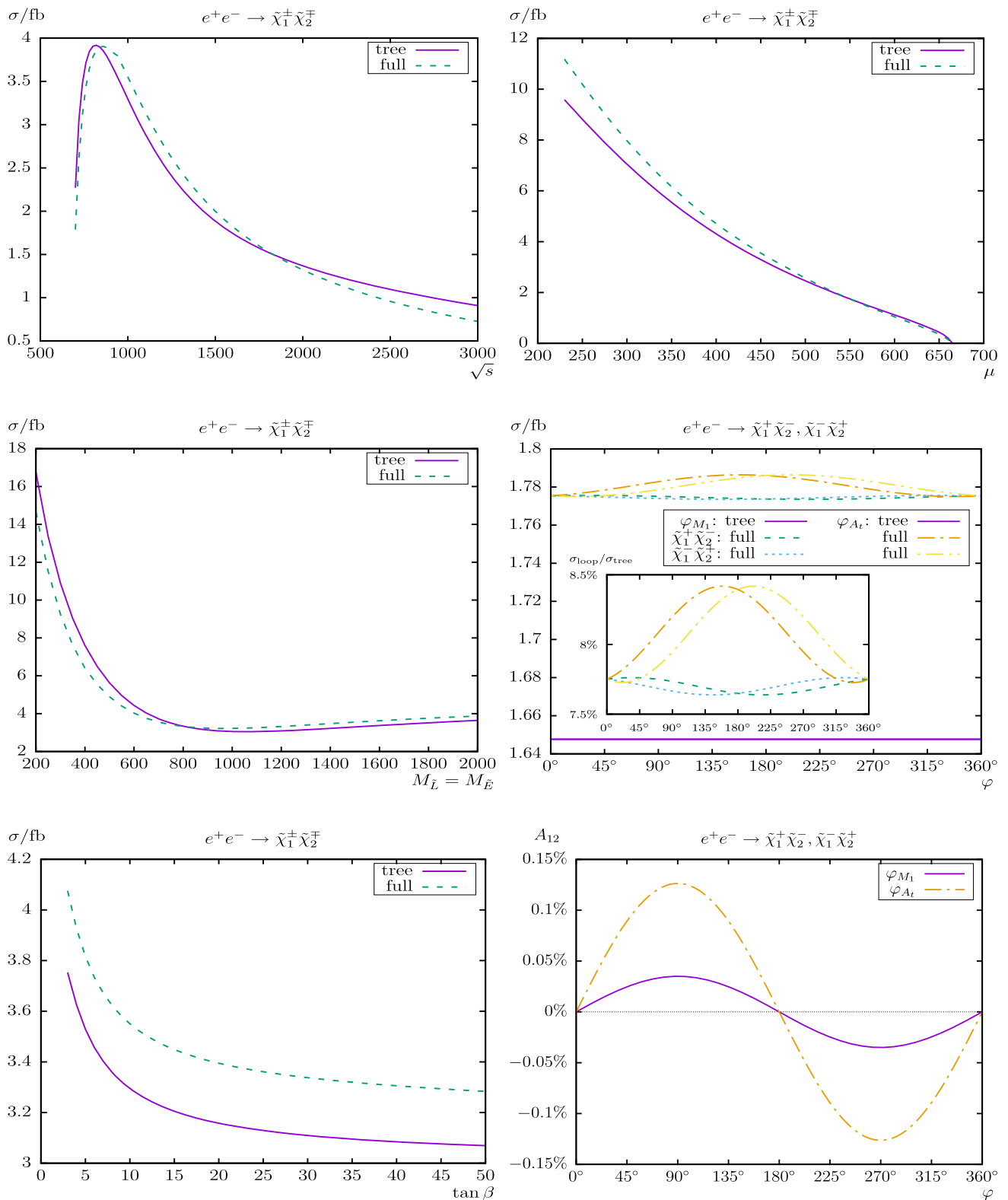


**Fig. 15**  $\sigma(e^+e^- \rightarrow \tilde{\chi}_1^\pm \tilde{\chi}_2^\mp)$ . Tree-level and full one-loop corrected cross sections are shown with parameters chosen according to  $\mathcal{S}$ ; see Table 2. The upper plots show the cross sections with  $\sqrt{s}$  (left) and  $\mu$  (right) varied; the middle plots show  $M_{\tilde{L}} = M_{\tilde{E}}$  (left) and  $\varphi_{M_1}, \varphi_{A_t}$

(right) varied; the lower plot the variation with  $t_\beta$  (left) and the  $\mathcal{CP}$ -odd observable  $A_{12}$  (right) varied with the complex phases  $\varphi_{M_1}$  and  $\varphi_{A_t}$ . All masses and energies are in GeV

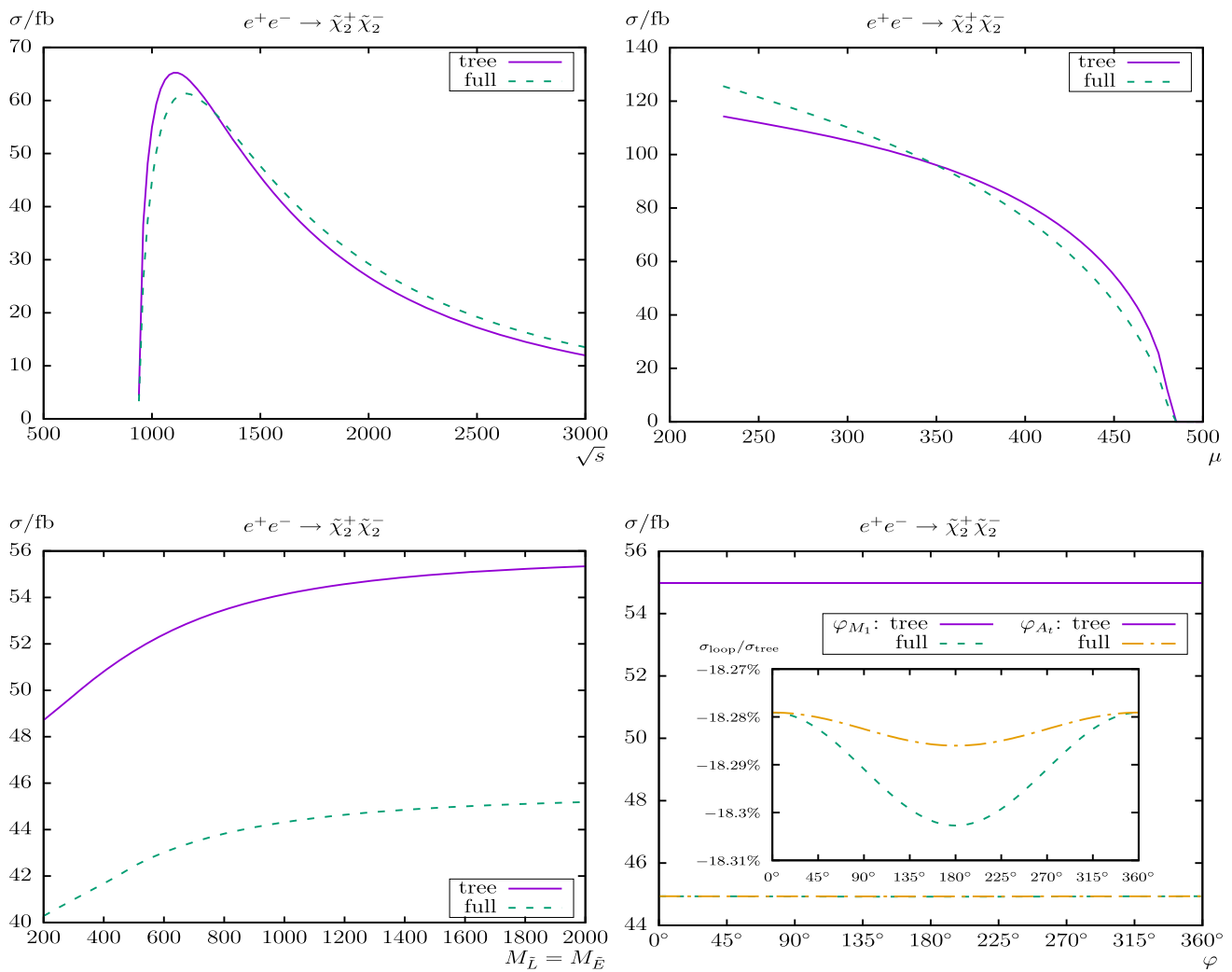


**Fig. 16**  $\sigma(e^+e^- \rightarrow \tilde{\chi}_2^+ \tilde{\chi}_2^-)$ . Tree-level and full one-loop corrected cross sections are shown with parameters chosen according to  $\mathcal{S}$ ; see Table 2. The upper plots show the cross sections with  $\sqrt{s}$  (left) and  $\mu$  (right) varied; the lower plots show  $M_{\tilde{L}} = M_{\tilde{E}}$  (left) and  $\varphi_{M_1}, \varphi_{A_i}$  (right) varied

turns out to be substantially larger than the effects of  $\varphi_{M_1}$ . They are found at the level of  $\sim +0.7\%$ , most likely below the level of observation.

For this production channel we also show the variation with  $t_\beta$  in the lower left plot of Fig. 15. From  $t_\beta \approx 3$  and  $\sigma(e^+e^- \rightarrow \tilde{\chi}_1^\pm \tilde{\chi}_2^\mp) \sim 4.1$  fb the cross section decreases to  $\sigma(e^+e^- \rightarrow \tilde{\chi}_1^\pm \tilde{\chi}_2^\mp) \sim 3.3$  fb at  $t_\beta = 50$ . The size of the loop corrections varies from  $\sim +8.6$  to  $\sim +7\%$  from low to high  $t_\beta$ .

In addition, here we show in the lower right plot of Fig. 15 the  $\mathcal{CP}$ -odd observable  $A_{12}$ ; see Eq. (7), varied with the complex phases  $\varphi_{M_1}$  and  $\varphi_{A_i}$ . However, for our parameter set  $\mathcal{S}$  the  $\mathcal{CP}$  asymmetries turn out to be very small, well below  $\pm 1\%$ , hardly measurable in future  $e^+e^-$  collider experiments.

We finish the  $e^+e^- \rightarrow \tilde{\chi}_c^\pm \tilde{\chi}_{c'}^\mp$  analysis in Fig. 16 in which the results for  $c = c' = 2$  are displayed. As a function

of  $\sqrt{s}$  (upper left plot) we find a maximum of  $\sim 60$  fb at  $\sqrt{s} = 1200$  GeV. The loop corrections are  $\sim -19\%$  at  $\sqrt{s} = 1000$  GeV (i.e.  $\mathcal{S}$ ), and  $\sim +13\%$  at  $\sqrt{s} = 3000$  GeV.

In  $\mathcal{S}$ , but with  $\mu$  varied (upper right plot) we find the highest values of  $\sim 125$  fb at the lowest mass scales, going to zero for  $\mu \approx 480$  GeV due to kinematics. The relative corrections are  $\sim +10\%$  at  $\mu = 240$  GeV and  $\sim -19\%$  at  $\mu = 450$  GeV (i.e.  $\mathcal{S}$ ), with a tree crossing at  $\mu \approx 350$  GeV.

The cross section increases slowly with increasing  $M_{\tilde{L}}$  and the full corrections reach their maximum of  $\sim 45$  fb at the highest values shown,  $M_{\tilde{L}} = 2000$  GeV. The relative corrections are nearly constant, increasing only from  $\sim -17.3\%$  at  $M_{\tilde{L}} = 200$  GeV to  $\sim -18.4\%$  at  $M_{\tilde{L}} = 2000$  GeV.

The dependence on  $\varphi_{M_1}$  and  $\varphi_{A_i}$  (lower right plot) is again tiny, the loop corrections are found to be nearly independent of  $\varphi_{M_1}$  and  $\varphi_{A_i}$  below the level of  $\sim +0.1\%$ , as shown explicitly in the inset.

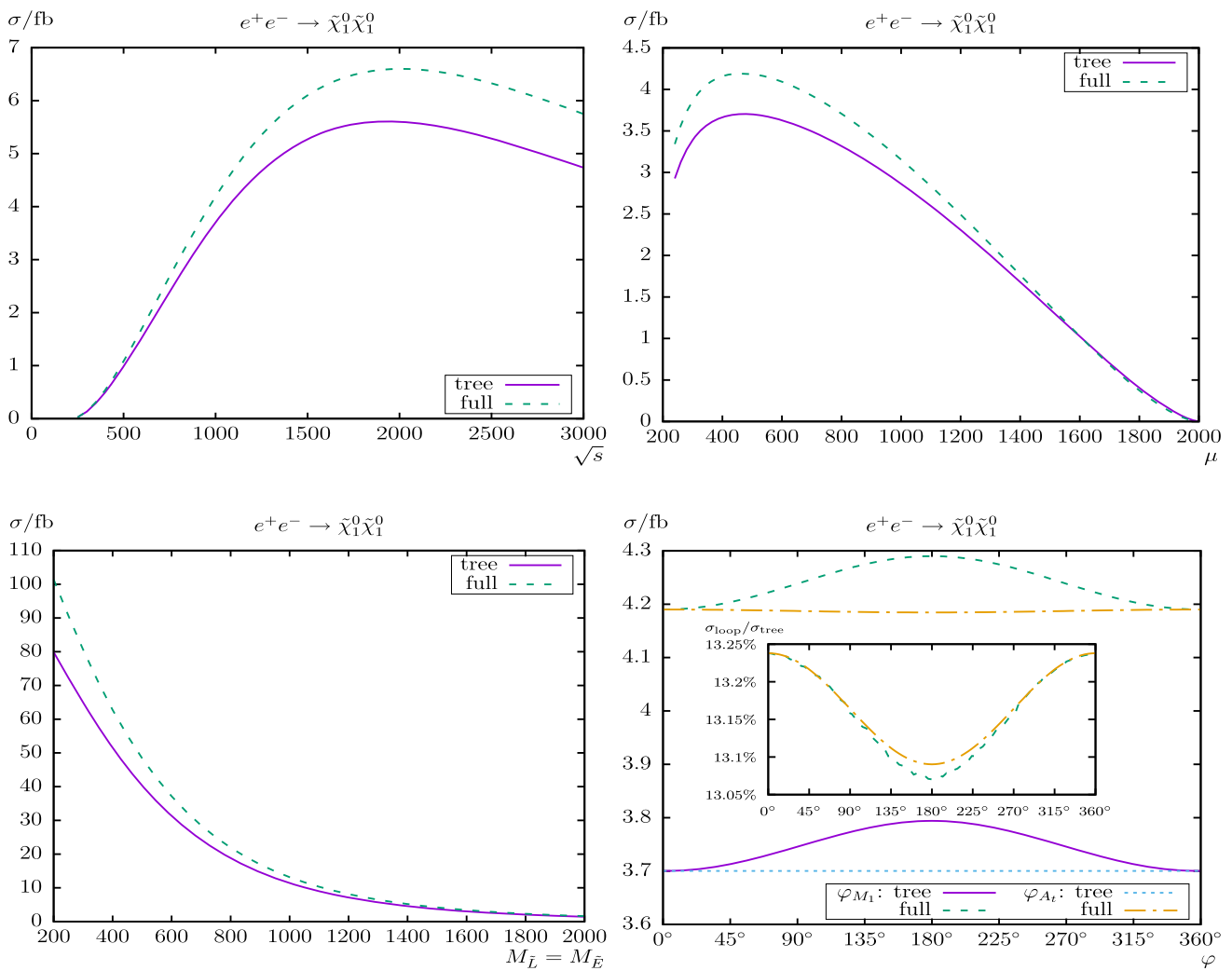


**Fig. 17**  $\sigma(e^+e^- \rightarrow \tilde{\chi}_1^0 \tilde{\chi}_1^0)$ . Tree-level and full one-loop corrected cross sections are shown with parameters chosen according to  $\mathcal{S}$ ; see Table 2. The upper plots show the cross sections with  $\sqrt{s}$  (left) and  $\mu$  (right) varied; the lower plots show  $M_{\tilde{L}} = M_{\tilde{E}}$  (left) and  $\varphi_{M_1}, \varphi_{A_t}$  (right) varied

Overall, for the chargino pair production we observed a decreasing cross section  $\propto 1/s$  for  $s \rightarrow \infty$ ; see Ref. [30]. The full one-loop corrections are very roughly 10–20% of the tree-level results, but depend strongly on the size of  $\mu$ , where larger values result even in negative loop corrections. The cross sections are largest for  $e^+e^- \rightarrow \tilde{\chi}_1^+ \tilde{\chi}_1^-$  and  $e^+e^- \rightarrow \tilde{\chi}_2^+ \tilde{\chi}_2^-$  and roughly smaller by one order of magnitude for  $e^+e^- \rightarrow \tilde{\chi}_1^\pm \tilde{\chi}_2^\mp$ . This is because there is no  $\gamma \tilde{\chi}_1^\pm \tilde{\chi}_2^\mp$  coupling at tree level in the MSSM. The variation of the cross sections and of the  $\mathcal{CP}$  asymmetry  $A_{12}$  with  $\varphi_{M_1}$  or  $\varphi_{A_t}$  is found extremely small and the dependence on other phases were found to be roughly at the same level and have not been shown explicitly.

### 4.3 The process $e^+e^- \rightarrow \tilde{\chi}_n^0 \tilde{\chi}_{n'}^0$

In Figs. 17, 18, 19, 20, 21, 22, 23, 24, 25 and 26 we show the results for the processes  $e^+e^- \rightarrow \tilde{\chi}_n^0 \tilde{\chi}_{n'}^0$  ( $n, n' = 1, 2, 3, 4$ )

as before as a function of  $\sqrt{s}$ ,  $\mu$ ,  $M_{\tilde{L}} = M_{\tilde{E}}$  and  $\varphi_{M_1}$ . It should be noted that for  $s \rightarrow \infty$  decreasing cross sections  $\propto 1/s$  are expected; see Ref. [31]. If not indicated otherwise, unpolarized electrons and positrons are assumed.

We start with the process  $e^+e^- \rightarrow \tilde{\chi}_1^0 \tilde{\chi}_1^0$  shown in Fig. 17. Away from the production threshold, loop corrections of  $\sim +13\%$  at  $\sqrt{s} = 1000$  GeV are found in scenario  $\mathcal{S}$  (see Table 2), with a maximum of nearly 7 fb at  $\sqrt{s} \approx 2000$  GeV. The relative size of the loop corrections increase with increasing  $\sqrt{s}$  and reach  $\sim +22\%$  at  $\sqrt{s} = 3000$  GeV.

With increasing  $\mu$  in  $\mathcal{S}$  (upper right plot) we find a strong decrease of the production cross section, as can be expected from kinematics, discussed above. The relative loop corrections reach  $\sim +14\%$  at  $\mu = 240$  GeV (at the border of the experimental exclusion bounds) and  $\sim +13\%$  at  $\mu = 450$  GeV (i.e.  $\mathcal{S}$ ). The tree crossing takes place at  $\mu \approx 1600$  GeV. For higher  $\mu$  values the loop corrections

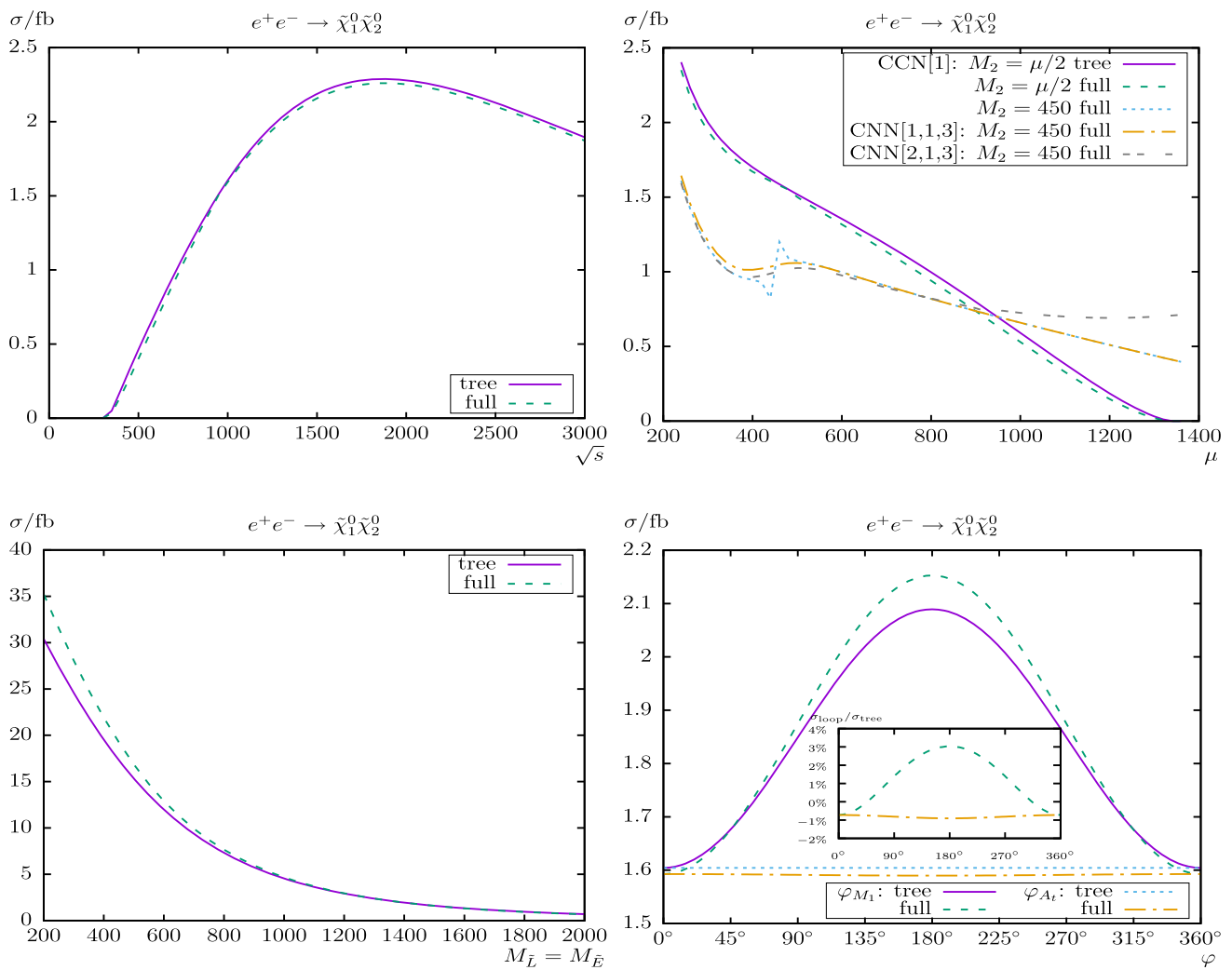


**Fig. 18**  $\sigma(e^+e^- \rightarrow \tilde{\chi}_1^0 \tilde{\chi}_2^0)$ . Tree-level and full one-loop corrected cross sections are shown with parameters chosen according to  $\mathcal{S}$ ; see Table 2. The upper plots show the cross sections with  $\sqrt{s}$  (left) and  $\mu$  (right) varied; the lower plots show  $M_{\tilde{L}} = M_{\tilde{E}}$  (left) and  $\varphi_{M_1}, \varphi_{A_t}$  (right) varied

are negative, where the relative size becomes large due to the (relative) smallness of the tree-level results, which goes to zero for  $\mu \approx 2000$  GeV.

The cross sections are decreasing with increasing  $M_{\tilde{L}}$ , i.e. the (negative) interference of the  $t$ -channel exchange decreases the cross sections, and the full one-loop result has its maximum of  $\sim 100$  fb at  $M_{\tilde{L}} = 200$  GeV. Analogously the relative corrections are decreasing from  $\sim +27\%$  at  $M_{\tilde{L}} = 200$  GeV to  $\sim +12\%$  at  $M_{\tilde{L}} = 2000$  GeV. For the other parameter variations one can conclude that a cross section larger by nearly one order of magnitude can be possible for very low  $M_{\tilde{L}}$  (which are not yet excluded experimentally).

Now we turn to the complex phase dependence. As for the chargino production,  $\varphi_{A_t}$  enters only via final state vertex corrections. On the other hand,  $\varphi_{M_1}$  enters already at tree level, and correspondingly larger effects are expected. We find that the phase dependence  $\varphi_{M_1}$  of the cross section in  $\mathcal{S}$  is

small (lower right plot), possibly not completely negligible, amounting up to  $\sim 2.3\%$  for the full corrections. The loop corrections at the level of  $\sim +13\%$  are found to be nearly independent of  $\varphi_{M_1}$ , with a relative variation of  $\sigma_{\text{loop}}/\sigma_{\text{tree}}$  at the level of  $\sim +0.2\%$ , (see the inlay in the lower right plot of Fig. 17). The loop effects of  $\varphi_{A_t}$  are found at the same level as the ones of  $\varphi_{M_1}$ , i.e. rather negligible.

The relative corrections for the process  $e^+e^- \rightarrow \tilde{\chi}_1^0 \tilde{\chi}_2^0$ , as shown in Fig. 18, are rather small for the parameter set chosen; see Table 2. In the upper left plot of Fig. 18 the peak (hardly visible in the dotted line) at  $\sqrt{s} \approx 940$  GeV is again the production threshold  $m_{\tilde{\chi}_1^\pm} + m_{\tilde{\chi}_2^\pm} = \sqrt{s}$ . The relative corrections are quasi-constant below  $\sim -2\%$  for  $\sqrt{s} \gtrsim 1000$  GeV.

The dependence on  $\mu$  with  $M_2 = \mu/2$  is shown in the upper right plot (the case of  $M_2 = 450$  GeV and the CNN  $[c, n, n']$  renormalization schemes are discussed

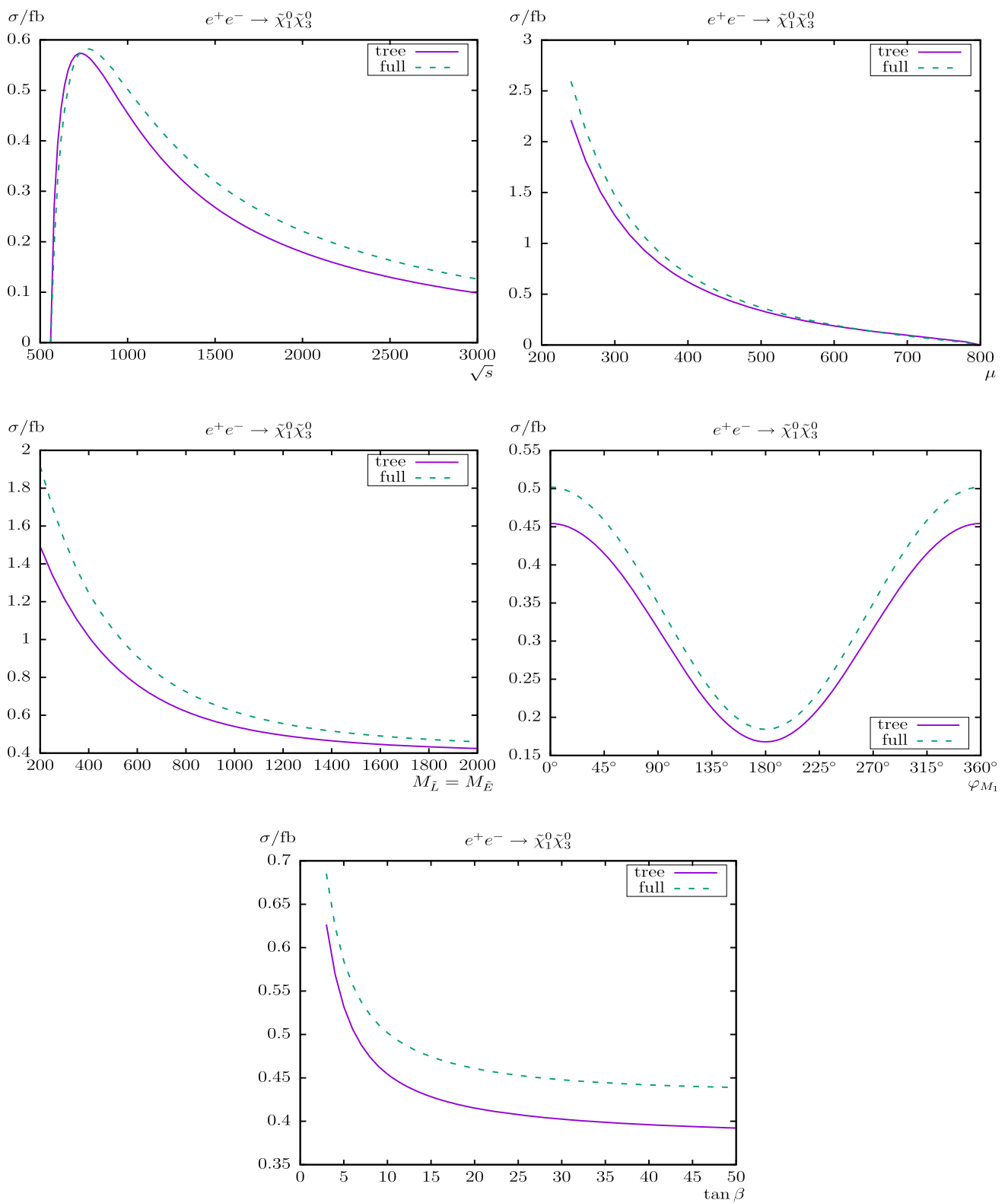


**Fig. 19**  $\sigma(e^+e^- \rightarrow \tilde{\chi}_1^0 \tilde{\chi}_3^0)$ . Tree-level and full one-loop corrected cross sections are shown with parameters chosen according to  $\mathcal{S}$ ; see Table 2. The upper plots show the cross sections with  $\sqrt{s}$  (left) and  $\mu$  (right) varied; the middle plots show  $M_{\tilde{L}} = M_{\tilde{E}}$  (left) and  $\varphi_{M_1}$  (right) varied; the lower plot shows the variation with  $\tan \beta$

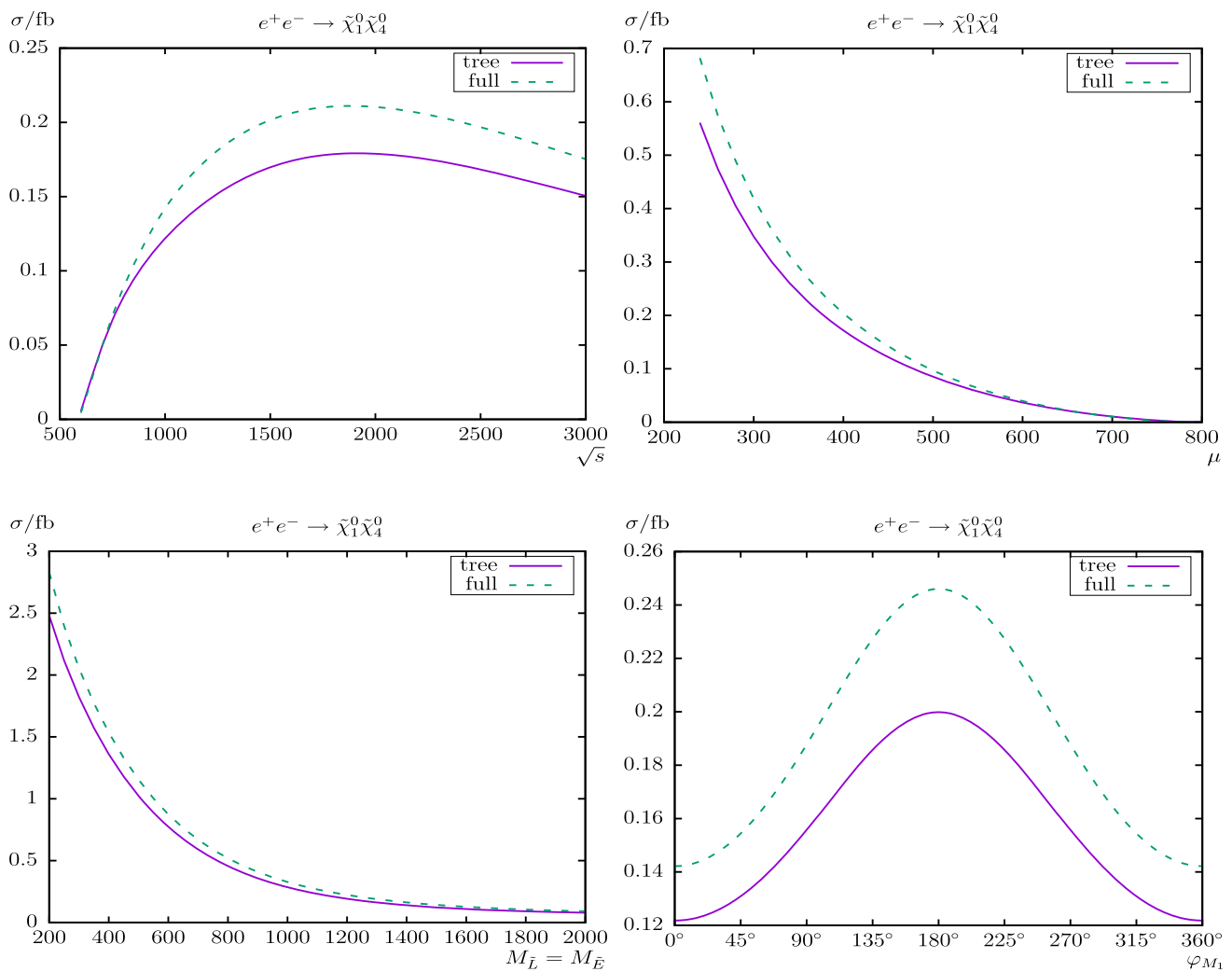


**Fig. 20**  $\sigma(e^+e^- \rightarrow \tilde{\chi}_1^0 \tilde{\chi}_4^0)$ . Tree-level and full one-loop corrected cross sections are shown with parameters chosen according to  $\mathcal{S}$ ; see Table 2. The upper plots show the cross sections with  $\sqrt{s}$  (left) and  $\mu$  (right) varied; the lower plots show  $M_{\tilde{L}} = M_{\tilde{E}}$  (left) and  $\varphi_{M_1}$  (right) varied

below). It is nearly linear and decreasing from  $\sim 2.4$  fb at small  $\mu$  down to zero at  $\mu \approx 1350$  GeV due to kinematics. The peak (hardly visible in the dotted line) at  $\mu \approx 481$  GeV is the production threshold  $m_{\tilde{\chi}_2^\pm} + m_{\tilde{\chi}_2^\pm} \approx \sqrt{s} = 1000$  GeV. The relative corrections are  $\sim -2\%$  at  $\mu = 230$  GeV and  $\sim -1\%$  at  $\mu = 450$  GeV (i.e.  $\mathcal{S}$ ).

The dependence on  $M_{\tilde{L}}$  is shown in the lower left plot of Fig. 18 and follows the same pattern as for  $e^+e^- \rightarrow \tilde{\chi}_1^0 \tilde{\chi}_1^0$ , i.e. a strong decrease with increasing  $M_{\tilde{L}}$ . Also in this case for the other parameter variations an order of magnitude increase could be possible for very low  $M_{\tilde{L}}$ .

The phase dependence  $\varphi_{M_1}$  of the cross section in  $\mathcal{S}$  is shown in the lower right plot of Fig. 18. In this case it turns out to be substantial, changing the full cross section by up to 26%. The tree crossings are at  $\varphi_{M_1} \approx 45^\circ, 315^\circ$ . The relative loop corrections ( $\sigma_{\text{loop}}/\sigma_{\text{tree}}$ ) vary with  $\varphi_{M_1}$  between  $\sim -0.7$  and  $\sim +3\%$ . The variation with  $\varphi_{A_1}$ , on the other hand, is

substantially smaller. The loop corrected cross section varies by less than  $-1\%$ , as can be seen in the inset.

Finally, in addition we have calculated the process  $e^+e^- \rightarrow \tilde{\chi}_1^0 \tilde{\chi}_2^0$  also within the CNN [1, 1, 3], CNN [1, 1, 4], CNN [2, 1, 2], and CNN [2, 1, 3] renormalization schemes; see Ref. [58]. The differences (compared to the CCN [1] scheme including our default choice of  $M_2 = \mu/2$ ) for all parameters  $\sqrt{s}$ ,  $\mu$ ,  $M_{\tilde{L}}$ , and  $\varphi_{M_1}$  varied with our input parameter set  $\mathcal{S}$  are very small (far below 1%). The only exception here is the CNN [2, 1, 3] renormalization scheme, where for  $\mu > 1000$  GeV we found a slightly larger difference of  $\sim 1\%$ . Because of these very small differences (within  $\mathcal{S}$ ) we have omitted to show the results for the CNN [c, n, n'] schemes in our Fig. 18.

In order to analyze the differences between the various renormalization schemes in more detail, we evaluated the process  $e^+e^- \rightarrow \tilde{\chi}_1^0 \tilde{\chi}_2^0$  for a slightly different parame-

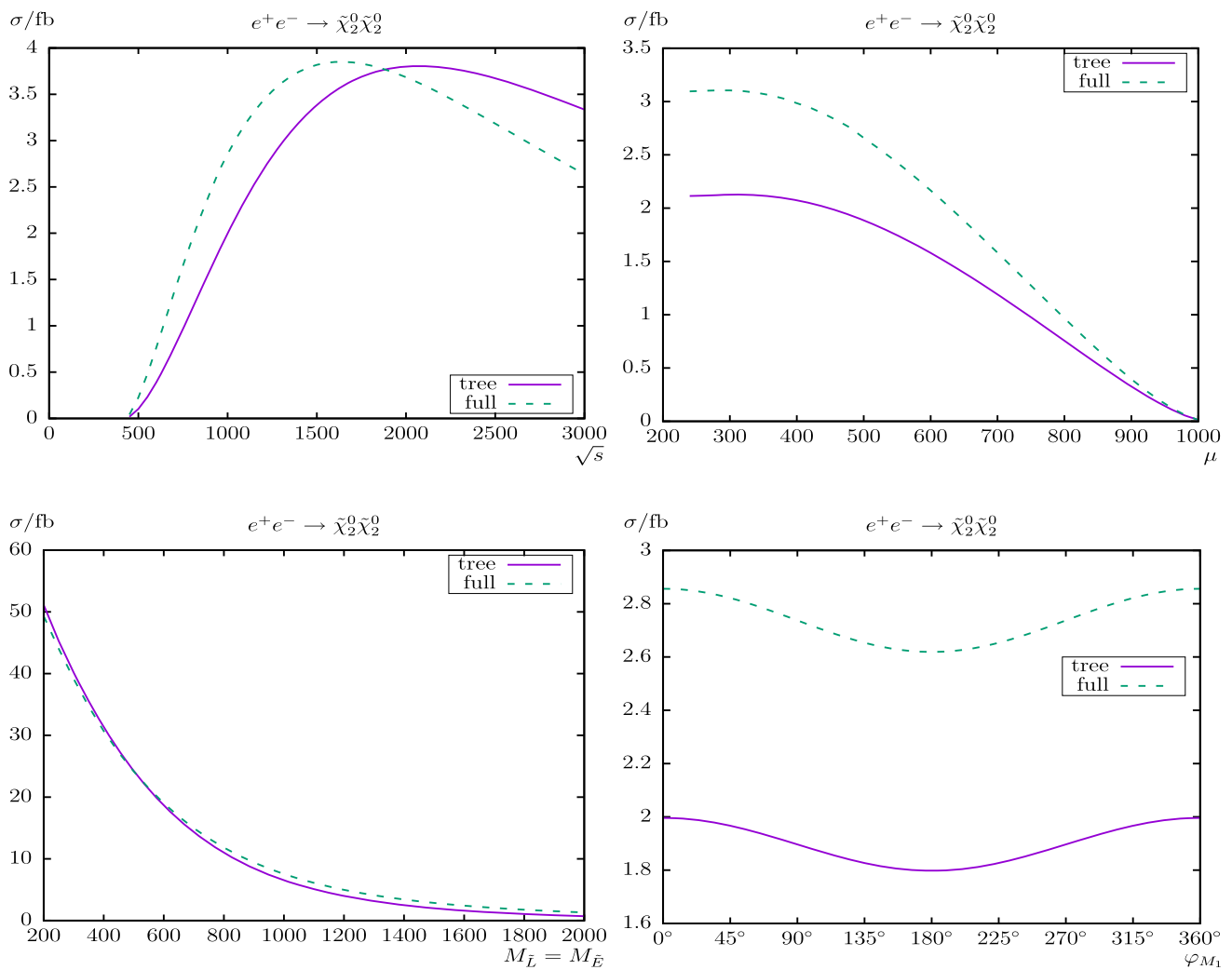


**Fig. 21**  $\sigma(e^+e^- \rightarrow \tilde{\chi}_2^0 \tilde{\chi}_2^0)$ . Tree-level and full one-loop corrected cross sections are shown with parameters chosen according to  $\mathcal{S}$ ; see Table 2. The upper plots show the cross sections with  $\sqrt{s}$  (left) and  $\mu$  (right) varied; the lower plots show  $M_{\tilde{L}} = M_{\tilde{E}}$  (left) and  $\varphi_{M_1}$  (right) varied

ter set with fixed  $M_2 = 450$  GeV and  $\mu$  varied. In the upper right plot of Fig. 18 the corresponding results are shown for the CCN[1], CCN[1, 1, 3], and CCN[2, 1, 3] schemes.<sup>9</sup> One can clearly see the expected breakdown of the CCN[1] scheme for  $\mu \approx M_2$ , i.e. in our case at  $\mu \approx M_2 = 450$  GeV (see also Refs. [27, 28]) and the smooth behavior of CCN[1, 1, 3] and CCN[2, 1, 3] around  $\mu \sim M_2 = 450$  GeV. Outside the region of  $\mu \sim M_2$  the scheme CCN[1] is expected to be reliable, since each of the three OS conditions is strongly connected to one of the three input parameters,  $M_1$ ,  $M_2$  and  $\mu$ . Similarly, CCN[2, 1, 3] (CCN[1, 1, 3]) is expected to be reliable for  $\mu$  smaller

(larger) than  $M_2$ , as in this case again each of the three OS renormalization conditions is strongly connected to the three input parameters. Exactly this behavior can be observed in the plot: for  $\mu \leq M_2 = 450$  GeV CCN[2, 1, 3] is nearly identical to CCN[1], whereas for  $\mu > M_2 = 450$  GeV the other scheme, CCN[1, 1, 3], is very close to CCN[1]. A rising deviation of the CCN[2, 1, 3] scheme from the other two schemes can be observed for  $\mu > 1000$  GeV. Here the fact contributes that we have an increasing mass splitting of the one-loop corrected masses  $m_{\tilde{\chi}_2^0}^{\text{OS}}$  between these schemes in the kinematics.<sup>10</sup>

<sup>9</sup> In the CCN[2, 1, 2] scheme the mass splitting between the tree-level neutralino mass  $m_{\tilde{\chi}_3^0}$  and the one-loop corrected mass  $m_{\tilde{\chi}_3^0}^{\text{OS}}$  (see Eq. (5)) is larger than 200% for this special parameter set (i.e.  $M_2 = 450$  GeV) and therefore unreliable. The CCN[1, 1, 4] scheme is even worse and delivers a negative  $m_{\tilde{\chi}_3^0}^{\text{OS}}$ .

<sup>10</sup> It should also be noted that for  $\mu > 1092$  GeV within CCN[2, 1, 3] we find an (increasing) mass splitting between the tree  $m_{\tilde{\chi}_2^0}$  and corrected neutralino mass  $m_{\tilde{\chi}_2^0}^{\text{OS}}$  of  $>10\%$ , pointing to a rather unreliable scheme for this part of the parameter space.



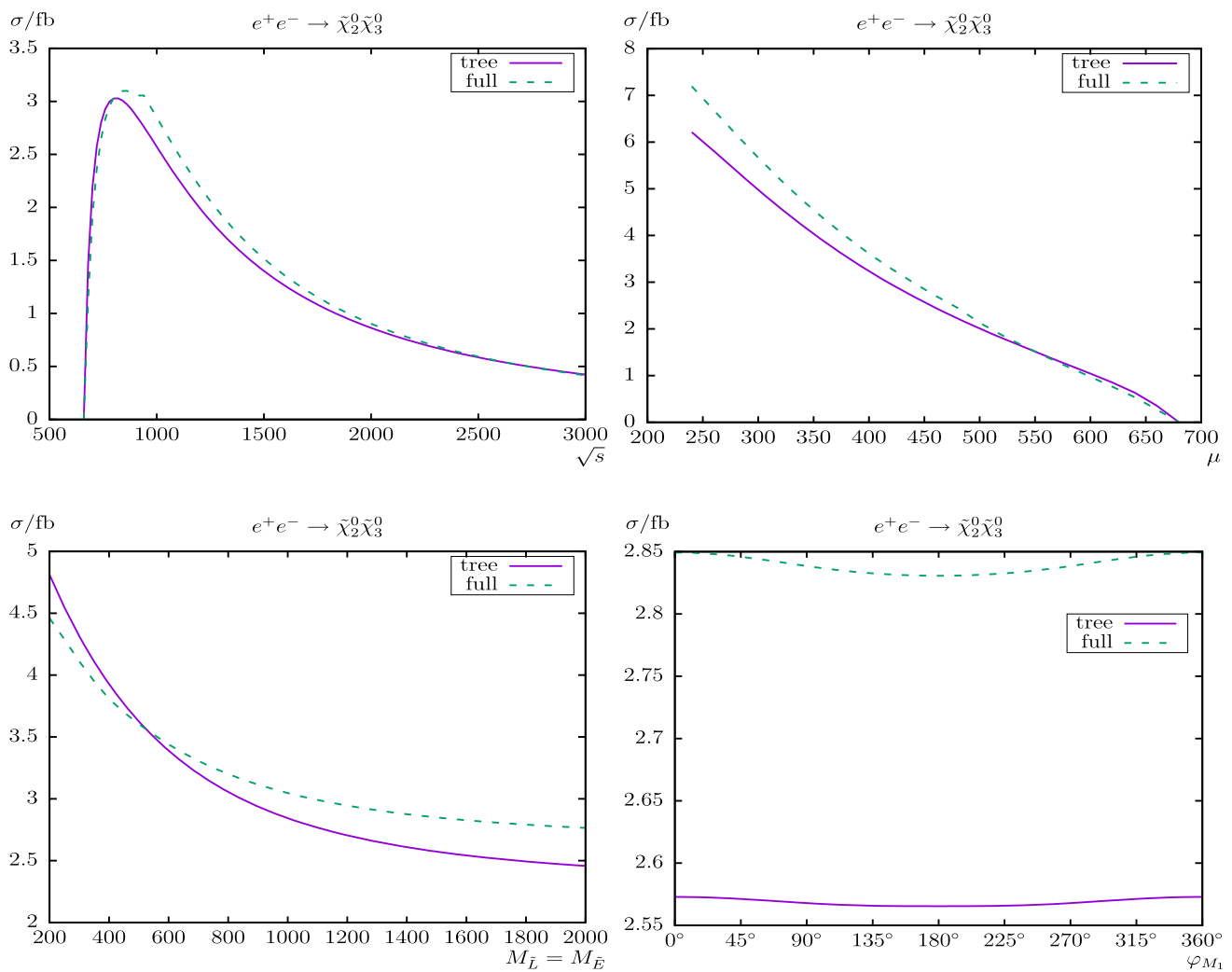


**Fig. 22**  $\sigma(e^+e^- \rightarrow \tilde{\chi}_2^0 \tilde{\chi}_3^0)$ . Tree-level and full one-loop corrected cross sections are shown with parameters chosen according to  $\mathcal{S}$ ; see Table 2. The upper plots show the cross sections with  $\sqrt{s}$  (left) and  $\mu$  (right) varied; the lower plots show  $M_{\tilde{L}} = M_{\tilde{E}}$  (left) and  $\varphi_{M_1}$  (right) varied

We now turn to the process  $e^+e^- \rightarrow \tilde{\chi}_1^0 \tilde{\chi}_3^0$  shown in Fig. 19, which is found to be rather small of  $\mathcal{O}(1 \text{ fb})$ . As a function of  $\sqrt{s}$  (upper row, left plot) we find a small shift w.r.t.  $\sqrt{s}$  directly at the production threshold, as well as a shift of  $\sim +50 \text{ GeV}$  of the maximum cross section position. The loop corrections range from  $\sim +11\%$  at  $\sqrt{s} = 1000 \text{ GeV}$  (i.e.  $\mathcal{S}$ ) to  $\sim +28\%$  at  $\sqrt{s} = 3000 \text{ GeV}$ .

The dependence on  $\mu$  (upper right plot) is rather small. The relative corrections are  $\sim +17\%$  at  $\mu = 240 \text{ GeV}$ ,  $\sim +11\%$  at  $\mu = 450 \text{ GeV}$  (i.e.  $\mathcal{S}$ ), and have a tree crossing at  $\mu \approx 650 \text{ GeV}$ . For larger  $\mu$  the cross section goes to zero due to kinematics.

The cross section decreases with  $M_{\tilde{L}}$  (middle left plot), again due to the negative interference of the  $t$ -channel contribution. The full correction has a maximum of  $\sim 2 \text{ fb}$  for  $M_{\tilde{L}} = 200 \text{ GeV}$ , going down to  $\sim 0.5 \text{ fb}$  at  $M_{\tilde{L}} = 2000 \text{ GeV}$ . Anal-

ogously the relative corrections are decreasing from  $\sim +28\%$  at  $M_{\tilde{L}} = 200 \text{ GeV}$  to  $\sim +8\%$  at  $M_{\tilde{L}} = 2000 \text{ GeV}$ .

The phase dependence  $\varphi_{M_1}$  of the cross section in  $\mathcal{S}$  is shown in the middle right plot of Fig. 19. It is very pronounced and can vary  $\sigma_{\text{full}}(e^+e^- \rightarrow \tilde{\chi}_1^0 \tilde{\chi}_3^0)$  by 60%. The (relative) loop corrections are at the level of  $\sim 10\%$  w.r.t. the tree cross section.

Here we also show the variation with  $t_\beta$  in the lower plot of Fig. 19. The loop corrected cross section decreases from  $\sim 0.7 \text{ fb}$  at small  $t_\beta$  to  $\sim 0.45 \text{ fb}$  at  $t_\beta = 50$ . The relative corrections for the  $t_\beta$  dependence are increasing from  $\sim +9\%$  at  $t_\beta = 3$  to  $\sim +12\%$  at  $t_\beta = 50$ .

The process  $e^+e^- \rightarrow \tilde{\chi}_1^0 \tilde{\chi}_4^0$  is shown in Fig. 20, which is found to be very small in  $\mathcal{S}$  at  $\mathcal{O}(0.1 \text{ fb})$ , but can be substantially larger by nearly one order of magnitude for small  $M_{\tilde{L}}$ ; see below. Away from the production threshold, loop correc-

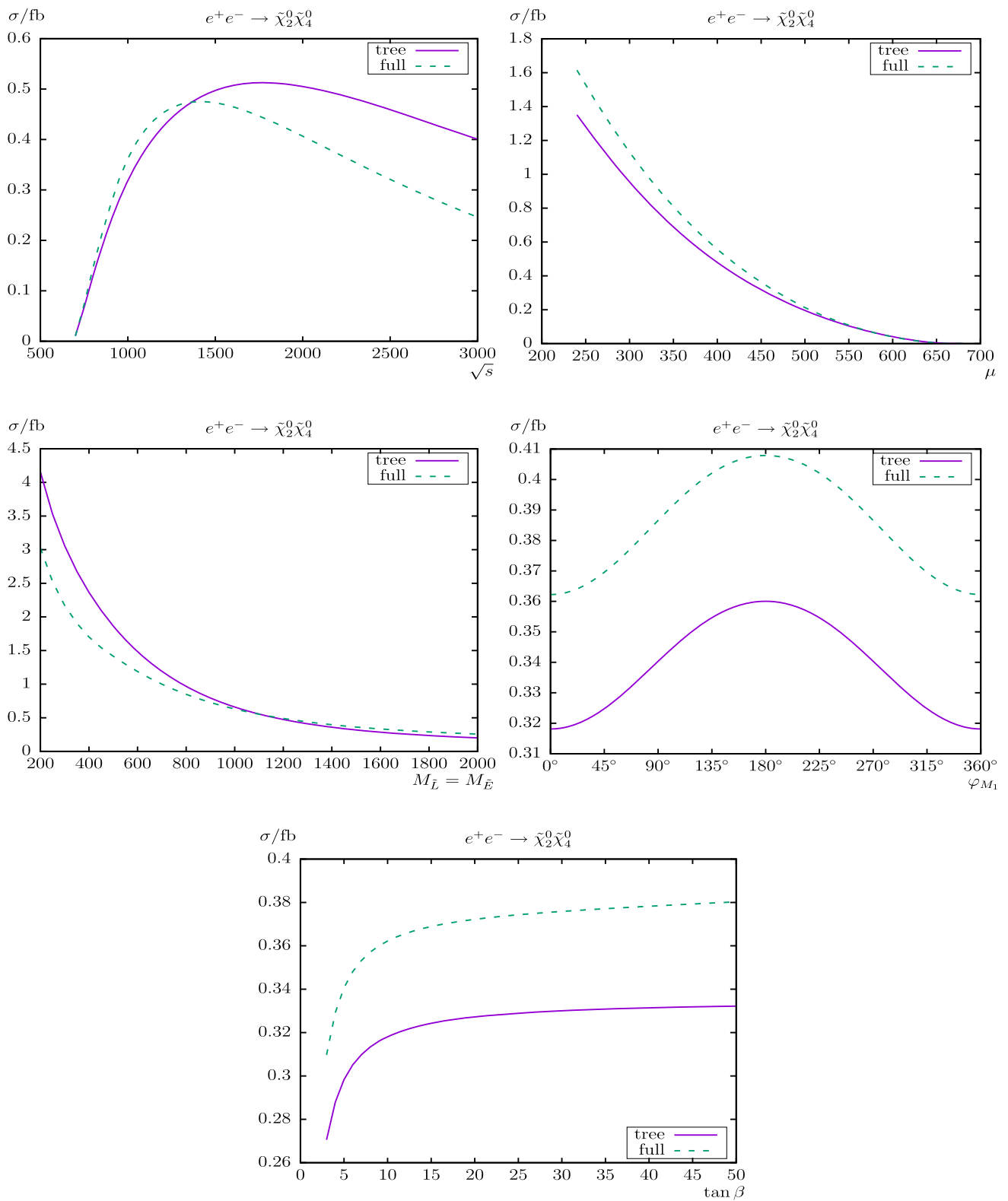


**Fig. 23**  $\sigma(e^+e^- \rightarrow \tilde{\chi}_2^0 \tilde{\chi}_4^0)$ . Tree-level and full one-loop corrected cross sections are shown with parameters chosen according to  $\mathcal{S}$ ; see Table 2. The upper plots show the cross sections with  $\sqrt{s}$  (left) and  $\mu$  (right) varied; the middle plots show  $M_{\tilde{L}} = M_{\tilde{E}}$  (left) and  $\varphi_{M_1}$  (right) varied, the lower plot shows the variation with  $\tan \beta$

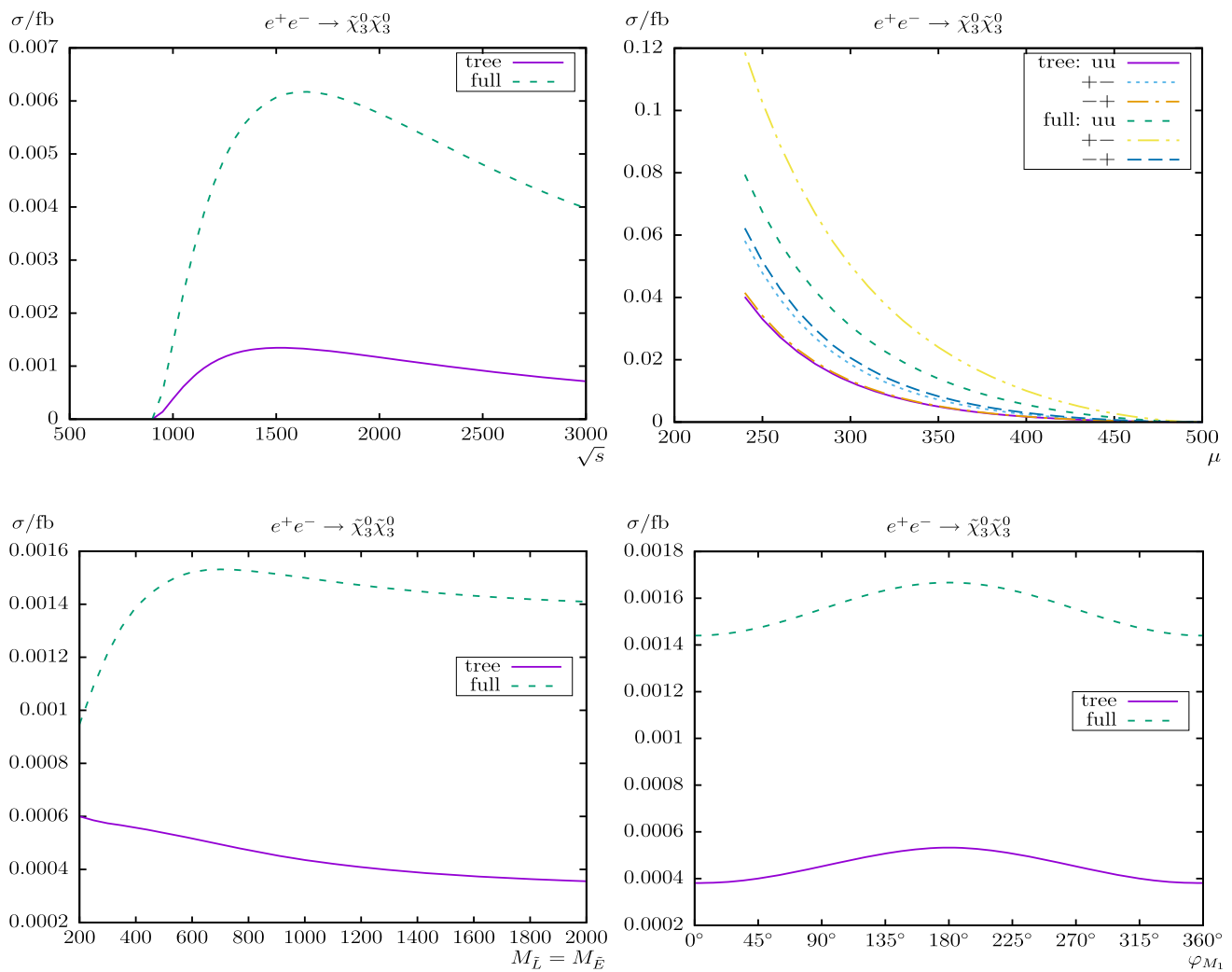


**Fig. 24**  $\sigma(e^+e^- \rightarrow \tilde{\chi}_3^0\tilde{\chi}_3^0)$ . Tree-level and full one-loop corrected cross sections are shown with parameters chosen according to  $\mathcal{S}$ ; see Table 2. The upper plots show the cross sections with  $\sqrt{s}$  (left) and  $\mu$

(right) varied; the lower plots show  $M_{\tilde{L}} = M_{\tilde{E}}$  (left) and  $\varphi_{M_1}$  (right) varied. The symbol u denotes unpolarized, + right-, and - left-circular polarized electrons and/or positrons (see text)

tions of  $\sim +17\%$  at  $\sqrt{s} = 1000$  GeV (i.e.  $\mathcal{S}$ ) are found. They reach their maximum of  $\sim +19\%$  at  $\sqrt{s} = 1250$  GeV and then decrease to  $\sim +16\%$  at  $\sqrt{s} = 3000$  GeV.

With increasing  $\mu$  in  $\mathcal{S}$  (upper right plot) we find again a decrease of the production cross section, as can be expected from kinematics. The relative loop corrections reach  $\sim +21\%$  at  $\mu = 240$  GeV and go down to  $\sim +17\%$  at  $\mu = 450$  GeV (i.e.  $\mathcal{S}$ ). The tree crossing is found at  $\mu \approx 700$  GeV, where the cross section is already below the observable level.

The cross section depends strongly on  $M_{\tilde{L}}$ . It is decreasing with increasing  $M_{\tilde{L}}$  and the full corrections have their maximum of  $\sim 2.8$  fb at  $M_{\tilde{L}} = 200$  GeV, going down to  $\sim 0.1$  fb at  $M_{\tilde{L}} = 2000$  GeV. The variation of the relative corrections are rather small,  $\sim +14\%$  at  $M_{\tilde{L}} = 200$  GeV,  $\sim +17\%$  at  $M_{\tilde{L}} = 1500$  GeV and  $\sim +14\%$  at  $M_{\tilde{L}} = 2000$  GeV.

The phase dependence on  $\varphi_{M_1}$  of the cross section in  $\mathcal{S}$  is shown in the lower right plot. The full cross section varies by more than 40%, and the (relative) loop corrections vary with  $\varphi_{M_1}$  between  $\sim +17$  and  $\sim +23\%$ , i.e. max.  $\sim +6\%$ .

The process  $e^+e^- \rightarrow \tilde{\chi}_2^0\tilde{\chi}_2^0$  is shown in Fig. 21. Away from the production threshold we find large loop corrections of  $\sim +43\%$  at  $\sqrt{s} = 1000$  GeV. The maximum cross section of nearly 4 fb is shifted from  $\sqrt{s} \approx 2100$  GeV down to  $\sqrt{s} \approx 1600$  GeV due to the full one-loop corrections. They have a tree crossing at  $\sqrt{s} \approx 1900$  GeV and reach  $\sim -20\%$  at  $\sqrt{s} = 3000$  GeV.

With increasing  $\mu$  in  $\mathcal{S}$  (upper right plot) we find a decrease of the production cross section, as can be expected from kinematics. The relative loop corrections also decrease from  $\sim +47\%$  at  $\mu = 240$  GeV to  $\sim +43\%$  at  $\mu = 450$  GeV

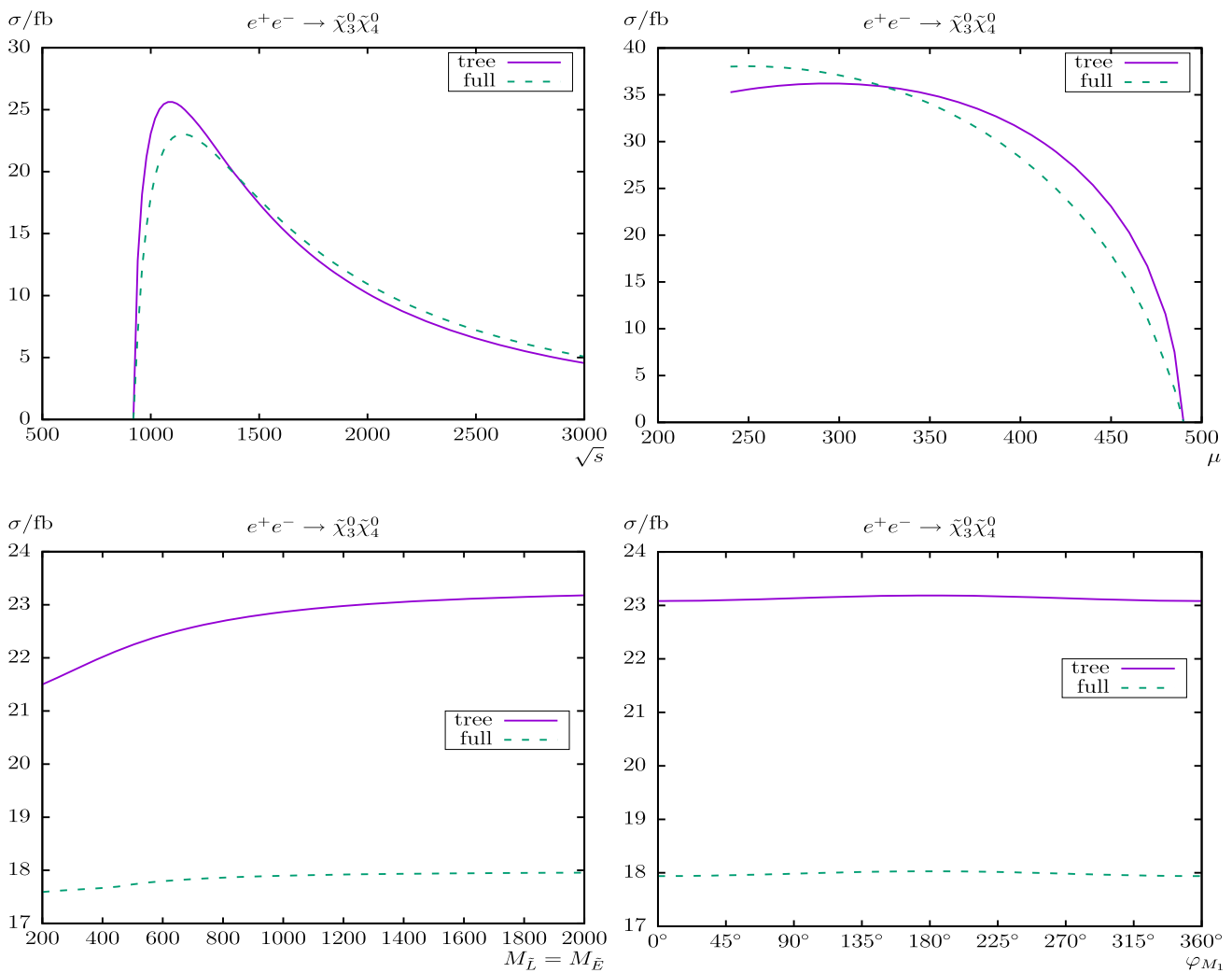


**Fig. 25**  $\sigma(e^+e^- \rightarrow \tilde{\chi}_3^0 \tilde{\chi}_4^0)$ . Tree-level and full one-loop corrected cross sections are shown with parameters chosen according to  $\mathcal{S}$ ; see Table 2. The upper plots show the cross sections with  $\sqrt{s}$  (left) and  $\mu$  (right) varied; the lower plots show  $M_{\tilde{L}} = M_{\tilde{E}}$  (left) and  $\varphi_{M_1}$  (right) varied

(i.e.  $\mathcal{S}$ ). The loop corrections go to zero for  $\mu = 1000$  GeV, where also the cross section goes to zero.

As for other neutralino production cross sections,  $\sigma(e^+e^- \rightarrow \tilde{\chi}_2^0 \tilde{\chi}_2^0)$  depends strongly on  $M_{\tilde{L}}$ , where values one order of magnitude larger than in  $\mathcal{S}$  with  $M_{\tilde{L}} = 1500$  GeV are possible for small  $M_{\tilde{L}}$ . One can see that the full corrections have their maximum of  $\sim 50$  fb at  $M_{\tilde{L}} = 200$  GeV. The relative corrections are increasing from  $\sim -3\%$  at  $M_{\tilde{L}} = 200$  GeV to  $\sim +84\%$  at  $M_{\tilde{L}} = 2000$  GeV with a tree crossing at  $M_{\tilde{L}} \approx 550$  GeV.

The phase dependence  $\varphi_{M_1}$  of the cross section in  $\mathcal{S}$  is shown in the lower right plot. The full cross section varies by  $\sim 7\%$ , where loop corrections are found at the level of  $\sim +43\%$  w.r.t. the tree cross section. The relative corrections ( $\sigma_{\text{loop}}/\sigma_{\text{tree}}$ ) vary up to  $\sim +2.5\%$  as a function of  $\varphi_{M_1}$ .

The dependence on  $t_\beta$  (not shown) is qualitatively similar to  $e^+e^- \rightarrow \tilde{\chi}_1^0 \tilde{\chi}_3^0$ . The relative corrections for the  $t_\beta$  depen-

dence are increasing from  $\sim +41\%$  at  $t_\beta = 3$  to  $\sim +44\%$  at  $t_\beta = 50$ .

Now we turn to the process  $e^+e^- \rightarrow \tilde{\chi}_2^0 \tilde{\chi}_3^0$  shown in Fig. 22. The peak in the upper left plot of Fig. 22 (in the dotted line) at  $\sqrt{s} \approx 940$  GeV is again the production threshold  $m_{\tilde{\chi}_2^\pm} + m_{\tilde{\chi}_3^\pm} = \sqrt{s}$ . As a function of  $\sqrt{s}$  we find relative corrections of  $\sim +11\%$  at  $\sqrt{s} = 1000$  GeV (i.e.  $\mathcal{S}$ ), and  $\sim -2\%$  at  $\sqrt{s} = 3000$  GeV with a tree crossing at  $\sqrt{s} \approx 2700$  GeV.

The dependence on  $\mu$  is shown in the upper right plot. The peak (hardly visible in the dotted line) at  $\mu \approx 481$  GeV is (again) the production threshold  $m_{\tilde{\chi}_2^\pm} + m_{\tilde{\chi}_3^\pm} \approx \sqrt{s} = 1000$  GeV. The relative corrections are  $\sim +16\%$  at  $\mu = 240$  GeV,  $\sim +11\%$  at  $\mu = 450$  GeV (i.e.  $\mathcal{S}$ ), and decreasing with a tree crossing for  $\mu \approx 550$  GeV. Due to kinematics the cross section goes to zero for  $\mu = 680$  GeV.

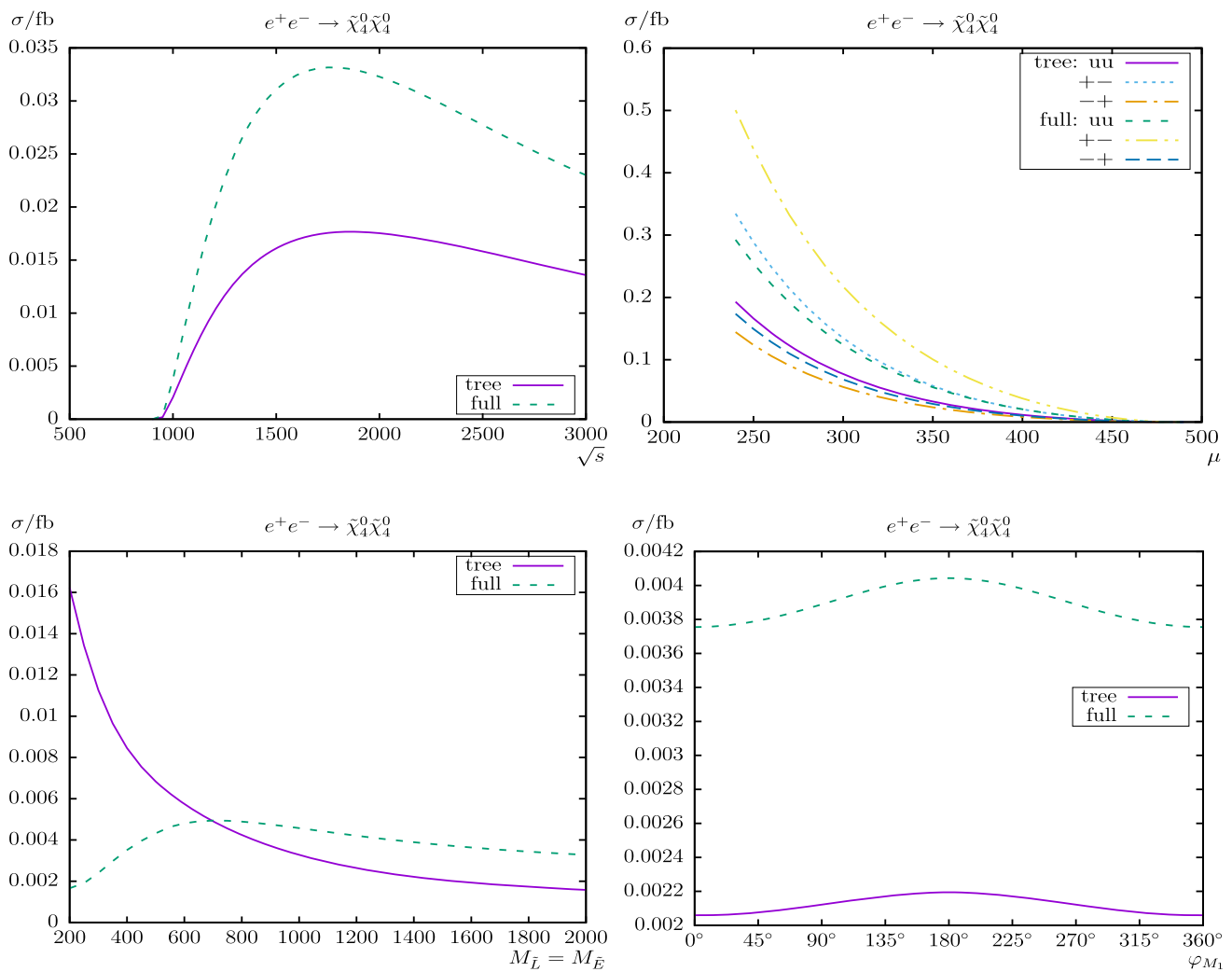


**Fig. 26**  $\sigma(e^+e^- \rightarrow \tilde{\chi}_4^0\tilde{\chi}_4^0)$ . Tree-level and full one-loop corrected cross sections are shown with parameters chosen according to  $\mathcal{S}$ ; see Table 2. The upper plots show the cross sections with  $\sqrt{s}$  (left) and  $\mu$

(right) varied; the lower plots show  $M_{\tilde{L}} = M_{\tilde{E}}$  (left) and  $\varphi_{M_1}$  (right) varied. u denotes unpolarized, + right-, and - left-circular polarized electrons and/or positrons (see text)

In the analysis as a function of  $M_{\tilde{L}}$  (lower row, left plot) the cross section is decreasing with increasing  $M_{\tilde{L}}$ , but varies (only) by a factor of  $\sim 2$  w.r.t.  $\mathcal{S}$ . The full correction has its maximum of  $\sim 4.5$  fb at  $M_{\tilde{L}} = 200$  GeV. The relative corrections are increasing from  $\sim -7\%$  at  $M_{\tilde{L}} = 200$  GeV to  $\sim +12\%$  at  $M_{\tilde{L}} = 2000$  GeV with a tree crossing at  $M_{\tilde{L}} \approx 520$  GeV.

The phase dependence  $\varphi_{M_1}$  of the cross section in  $\mathcal{S}$  is shown in the lower right plot of Fig. 22. The full cross section is found to vary at the per-cent level. The loop corrections are  $\sim 11\%$ , but the (relative) variation with  $\varphi_{M_1}$  stays below 0.4%.

The process  $e^+e^- \rightarrow \tilde{\chi}_2^0\tilde{\chi}_4^0$  is shown in Fig. 23 and is found to be rather small, where, as before, an increase by an order of magnitude is possible for low  $M_{\tilde{L}}$ ; see below. The peak in the upper left plot (not visible in the dotted line) at

$\sqrt{s} \approx 940$  GeV is (again) the production threshold  $m_{\tilde{\chi}_2^\pm} + m_{\tilde{\chi}_4^\pm} = \sqrt{s}$ . As a function of  $\sqrt{s}$  we find loop corrections of  $\sim +14\%$  at  $\sqrt{s} = 1000$  GeV (i.e.  $\mathcal{S}$ ), a tree crossing at  $\sqrt{s} \approx 1400$  GeV and  $\sim -38\%$  at  $\sqrt{s} = 3000$  GeV.

The dependence on  $\mu$  is shown in the upper right plot. The peak (not visible in the dotted line) at  $\mu \approx 481$  GeV is (again) the production threshold  $m_{\tilde{\chi}_2^\pm} + m_{\tilde{\chi}_4^\pm} \approx \sqrt{s} = 1000$  GeV. The relative corrections are  $\sim +20\%$  at  $\mu = 240$  GeV,  $\sim +14\%$  at  $\mu = 450$  GeV (i.e.  $\mathcal{S}$ ) and decrease further for larger  $\mu$ , crossing zero at  $\mu \approx 600$  GeV, where the cross section is below the observable level in  $\mathcal{S}$ .

In the analysis as a function of  $M_{\tilde{L}}$  (middle left plot) the cross sections are decreasing with increasing  $M_{\tilde{L}}$  and the full corrections have their maximum of  $\sim 3$  fb at  $M_{\tilde{L}} = 200$  GeV, about an order of magnitude larger than in  $\mathcal{S}$ . The relative corrections are changing from  $\sim -28\%$  at  $M_{\tilde{L}} = 200$  GeV

to  $\sim +28\%$  at  $M_{\tilde{L}} = 2000$  GeV with a tree crossing at  $M_{\tilde{L}} = 1100$  GeV.

The phase dependence  $\varphi_{M_1}$  of the cross section in  $\mathcal{S}$  is shown in the middle right plot of Fig. 23. The full correction is seen to vary up to  $\sim +12\%$  with loop corrections increasing the tree-level result by  $\sim +14\%$ . The phase dependence of the relative loop correction is (again) rather small and found to be below 0.6%.

We show again in the lower row the dependence on  $t_\beta$ . Contrary to other neutralino production cross sections analyzed before,  $\sigma_{\text{full}}(e^+e^- \rightarrow \tilde{\chi}_2^0 \tilde{\chi}_4^0)$  increases with  $t_\beta$  by up to  $\sim 21\%$  going from the lowest to the highest  $t_\beta$  values. The relative corrections for the  $t_\beta$  dependence vary below  $+0.8\%$ , between  $\sim +13.75\%$  at  $t_\beta = 17$  and  $\sim +14.5\%$  at  $t_\beta = 50$ .

The process  $e^+e^- \rightarrow \tilde{\chi}_3^0 \tilde{\chi}_3^0$  is shown in Fig. 24. The overall size of this cross section turns out to be very small, including all analyzed parameter variations. Consequently, the loop corrections have a sizable impact, as can be seen in all four panels of Fig. 24, but never lift the cross section above 0.08 fb. For this reason we refrain from a more detailed discussion here. However, we would like to remark that with polarized positrons ( $P(e^+) = +30\%$ ) and electrons ( $P(e^-) = -80\%$ ) cross sections up to  $\sim 0.1$  fb are possible in  $\mathcal{S}$ , as we show in the upper right plot. This could result in an observable cross section for some parts of the allowed parameter range; see Ref. [121] for related discussions.

We now turn to the process  $e^+e^- \rightarrow \tilde{\chi}_3^0 \tilde{\chi}_4^0$  shown in Fig. 25, which turns out to be sizable at the level of several 10 fb. As a function of  $\sqrt{s}$  (upper left plot) we find loop corrections of  $\sim -20\%$  at  $\sqrt{s} = 1000$  GeV (i.e.  $\mathcal{S}$ ), and  $\sim +11\%$  at  $\sqrt{s} = 3000$  GeV, with a tree crossing at  $\sqrt{s} \approx 1400$  GeV.

The dependence on  $\mu$  is shown in the upper right plot. The relative corrections are  $\sim +8\%$  at  $\mu = 240$  GeV,  $\sim -22\%$  at  $\mu = 450$  GeV (i.e.  $\mathcal{S}$ ), where the cross section goes to zero at  $\mu = 490$  GeV. The tree crossing is found at  $\mu \approx 320$  GeV.

In the analysis as a function of  $M_{\tilde{L}}$  (lower left plot) the cross section is nearly independent of  $M_{\tilde{L}}$ , due to the strong higgsino admixture of the final state neutralinos. This feature was already observable in Fig. 24. The loop corrected cross section is  $\sim 18$  fb. The relative corrections are increasing from  $\sim -18\%$  at  $M_{\tilde{L}} = 200$  GeV to  $\sim -23\%$  at  $M_{\tilde{L}} = 2$  TeV.

The phase dependence  $\varphi_{M_1}$  of the cross section in  $\mathcal{S}$  is shown in the lower right plot of Fig. 25 and is found to be negligible. This applies to the cross section as well as the absolute and the relative size of the loop corrections as a function of  $\varphi_{M_1}$ .

Finally we analyze the process  $e^+e^- \rightarrow \tilde{\chi}_4^0 \tilde{\chi}_4^0$ , shown in Fig. 26. Again as for  $e^+e^- \rightarrow \tilde{\chi}_3^0 \tilde{\chi}_3^0$  the overall size of this cross section is small,  $\mathcal{O}(10 \text{ ab})$ . This holds again for all parameter variations. For this reason we (again) skip a more detailed discussion here. Using polarized electrons/positrons ( $P(e^+) = +30\%$  and  $P(e^-) = -80\%$ ), as shown in the

upper right plot could yield production cross sections up to  $\sim 0.4$  fb, again possibly observable over some part of the relevant parameter space.

Overall, for the neutralino pair production the leading-order corrections can reach a level of  $\mathcal{O}(10 \text{ fb})$ , depending on the SUSY parameters, but is very small for the production of two equal higgsino dominated neutralinos at the  $\mathcal{O}(10 \text{ ab})$  level. This renders these processes difficult to observe at an  $e^+e^-$  collider.<sup>11</sup> Having both beams polarized could turn out to be crucial to yield a detectable production cross section in this case; see Ref. [121] for related analyses.

The full one-loop corrections are very roughly 10–20% of the tree-level results, but vary strongly on the size of  $\mu$  and  $M_{\tilde{L}}$ . Depending on the size of in particular these two parameters the loop corrections can be either positive or negative. This shows that the loop corrections, while being large, have to be included point-by-point in any precision analysis. The dependence on  $\varphi_{M_1}$  was found at the level of  $\sim 15\%$ , but can go up to  $\sim 40\%$  for the extreme cases. The relative loop corrections varied by up to 5% with  $\varphi_{M_1}$ . Consequently, the complex phase dependence must be taken into account as well.

## 5 Conclusions

We have evaluated all chargino/neutralino production modes at  $e^+e^-$  colliders with a two-particle final state, i.e.  $e^+e^- \rightarrow \tilde{\chi}_c^\pm \tilde{\chi}_{c'}^\mp$  and  $e^+e^- \rightarrow \tilde{\chi}_n^0 \tilde{\chi}_{n'}^0$  allowing for complex parameters. In the case of discovery of charginos and neutralinos a subsequent precision measurement of their properties will be crucial to determine their nature and the underlying (SUSY) parameters. In order to yield sufficient accuracy, one-loop corrections to the various chargino/neutralino production modes have to be considered. This is particularly the case for the anticipated high accuracy of the chargino/neutralino property determination at  $e^+e^-$  colliders [19].

The evaluation of the processes (1) and (2) is based on a full one-loop calculation, also including hard and soft QED radiation. The renormalization is chosen to be identical as for the various chargino/neutralino decay calculations; see, e.g., Refs. [25–28] or chargino/higgsino production from heavy Higgs-boson decay; see, e.g., Ref. [29]. Consequently, the predictions for the production and decay can be used together in a consistent manner (e.g., in a global phenomenological analysis of the chargino/neutralino sector at the one-loop level).

We first very briefly reviewed the relevant sectors including some details of the one-loop renormalization procedure

<sup>11</sup> The limit of 10 ab corresponds to ten events at an integrated luminosity of  $\mathcal{L} = 1 \text{ ab}^{-1}$ , which constitutes a guideline for the observability of a process at a linear collider.

of the cMSSM, which are relevant for our calculation. In most cases we follow Ref. [58]. We have discussed the calculation of the one-loop diagrams, the treatment of UV, IR, and collinear divergences that are canceled by the inclusion of (hard, soft, and collinear) QED radiation. As far as possible we have checked our result against the literature, and in most cases we found good agreement; parts of the differences can be attributed to problems with input parameters and/or different renormalization schemes (conversions).

For the analysis we have chosen a standard parameter set (see Table 2), which allows for the production of all combinations of charginos/neutralinos at an  $e^+e^-$  collider with a center-of-mass energy up to  $\sqrt{s} = 1000$  GeV. In the analysis we investigated the variation of the various production cross sections with the center-of-mass energy  $\sqrt{s}$ , the Higgs mixing parameter  $\mu$ , the slepton soft SUSY-breaking parameter  $M_{\tilde{L}}$  and the complex phases  $\varphi_{M_1}$  and  $\varphi_{A_t}$  of the gaugino mass parameter  $M_1$  and the trilinear Higgs-stop coupling,  $A_t$ , respectively. Where relevant we also showed the variation with  $t_\beta$ .

In our numerical scenarios we compared the tree-level production cross sections with the full one-loop corrected cross sections. The numerical results we have shown are, of course, dependent on the choice of the SUSY parameters. Nevertheless, they give an idea of the relevance of the full one-loop corrections. For the chargino pair production,  $e^+e^- \rightarrow \tilde{\chi}_c^\pm \tilde{\chi}_{c'}^\mp$ , we observed a decreasing cross section  $\propto 1/s$  for  $s \rightarrow \infty$ . The full one-loop corrections are very roughly 10–20% of the tree-level results but depend strongly on the size of  $\mu$ , where larger values result even in negative loop corrections. The cross sections are largest for  $e^+e^- \rightarrow \tilde{\chi}_1^+ \tilde{\chi}_1^-$  and  $e^+e^- \rightarrow \tilde{\chi}_2^+ \tilde{\chi}_2^-$  and roughly smaller by one order of magnitude for  $e^+e^- \rightarrow \tilde{\chi}_1^\pm \tilde{\chi}_2^\mp$  due to the absence of the  $\gamma \tilde{\chi}_1^\pm \tilde{\chi}_2^\mp$  coupling at tree level in the MSSM. The variation of the cross sections and of the  $\mathcal{CP}$  asymmetry  $A_{12}$  with  $\varphi_{M_1}$  or  $\varphi_{A_t}$  is found extremely small and the dependence on other phases were found to be roughly at the same level and have not been shown explicitly.

For the neutralino pair production,  $e^+e^- \rightarrow \tilde{\chi}_n^0 \tilde{\chi}_{n'}^0$ , the cross section can reach a level of  $\mathcal{O}(10 \text{ fb})$ , depending on the SUSY parameters, but is very small for the production of two equal higgsino dominated neutralinos at the  $\mathcal{O}(10 \text{ ab})$ . This renders these processes difficult to observe at an  $e^+e^-$  collider.<sup>12</sup> Having both beams polarized could turn out to be crucial to yield a detectable production cross section in this case. The full one-loop corrections are very roughly 10–20% of the tree-level results, but vary strongly on the size of  $\mu$  and  $M_{\tilde{L}}$ . Depending on the size of in particular these two parameters the loop corrections can be either positive or negative.

The dependence on  $\varphi_{M_1}$  was found to reach up to  $\sim 15\%$ , but can go up to  $\sim 40\%$  for the extreme cases. The (relative) loop corrections varied by up to 5% with  $\varphi_{M_1}$ . This shows that the loop corrections, including the complex phase dependence, have to be included point-by-point in any precision analysis, or any precise determination of (SUSY) parameters from the production of cMSSM charginos/neutralinos at  $e^+e^-$  linear colliders. We emphasize again that our full one-loop calculation can readily be used together with corresponding full one-loop corrections to chargino/neutralino decays [25–28] or other chargino/neutralino production modes [29].

**Acknowledgements** We thank A. Bharucha, T. Blank, T. Hahn and F. von der Pahlen for helpful discussions. The work of S.H. is supported in part by CICYT (Grant FPA 2013-40715-P), in part by the MEINCOOP Spain under contract FPA2016-78022-P, in part by the “Spanish Agencia Estatal de Investigación” (AEI) and the EU “Fondo Europeo de Desarrollo Regional” (FEDER) through the project FPA2016-78645-P, and by the Spanish MICINN’s Consolider-Ingenio 2010 Program under Grant MultiDark CSD2009-00064.

**Open Access** This article is distributed under the terms of the Creative Commons Attribution 4.0 International License (<http://creativecommons.org/licenses/by/4.0/>), which permits unrestricted use, distribution, and reproduction in any medium, provided you give appropriate credit to the original author(s) and the source, provide a link to the Creative Commons license, and indicate if changes were made. Funded by SCOAP<sup>3</sup>.

## References

1. H. Nilles, Phys. Rep. **110**, 1 (1984)
2. R. Barbieri, Riv. Nuovo Cim. **11**, 1 (1988)
3. H. Haber, G. Kane, Phys. Rep. **117**, 75 (1985)
4. J. Gunion, H. Haber, Nucl. Phys. B **272**, 1 (1986)
5. G. Aad et al., [ATLAS Collaboration], Phys. Lett. B **716**, 1 (2012). [arXiv:1207.7214](https://arxiv.org/abs/1207.7214) [hep-ex]
6. S. Chatrchyan et al., [CMS Collaboration], Phys. Lett. B **716**, 30 (2012). [arXiv:1207.7235](https://arxiv.org/abs/1207.7235) [hep-ex]
7. H. Goldberg, Phys. Rev. Lett. **50**, 1419 (1983)
8. J. Ellis, J. Hagelin, D. Nanopoulos, K. Olive, M. Srednicki, Nucl. Phys. B **238**, 453 (1984)
9. A. Pilaftsis, Phys. Rev. D **58**, 096010 (1998). [arXiv:hep-ph/9803297](https://arxiv.org/abs/hep-ph/9803297)
10. A. Pilaftsis, Phys. Lett. B **435**, 88 (1998). [arXiv:hep-ph/9805373](https://arxiv.org/abs/hep-ph/9805373)
11. D.A. Demir, Phys. Rev. D **60**, 055006 (1999). [arXiv:hep-ph/9901389](https://arxiv.org/abs/hep-ph/9901389)
12. A. Pilaftsis, C.E.M. Wagner, Nucl. Phys. B **553**, 3 (1999). [arXiv:hep-ph/9902371](https://arxiv.org/abs/hep-ph/9902371)
13. S. Heinemeyer, Eur. Phys. J. C **22**, 521 (2001). [arXiv:hep-ph/0108059](https://arxiv.org/abs/hep-ph/0108059)
14. H. Baer et al., The International Linear Collider Technical Design Report—volume 2: physics. [arXiv:1306.6352](https://arxiv.org/abs/1306.6352) [hep-ph]
15. R.-D. Heuer et al., [TESLA Collaboration], TESLA Technical Design Report, Part III: Physics at an  $e^+e^-$  Linear Collider. see [http://tesla.desy.de/new\\_pages/TDR\\_CD/start.html](http://tesla.desy.de/new_pages/TDR_CD/start.html). [arXiv:hep-ph/0106315](https://arxiv.org/abs/hep-ph/0106315)
16. K. Ackermann et al., in *Proceedings Summer Colloquium*, Amsterdam, Netherlands, 4 April 2003, DESY-PROC-2004-01

<sup>12</sup> The limit of 10 ab corresponds to ten events at an integrated luminosity of  $\mathcal{L} = 1 \text{ ab}^{-1}$ , which constitutes a guideline for the observability of a process at a linear collider.

17. J. Brau et al., [ILC Collaboration], ILC Reference Design Report volume 1—executive summary. [arXiv:0712.1950](#) [physics.acc-ph]
18. A. Djouadi et al., [ILC Collaboration], International Linear Collider Reference Design Report volume 2: physics at the ILC. [arXiv:0709.1893](#) [hep-ph]
19. G. Moortgat-Pick et al., *Eur. Phys. J. C* **75**(8), 371 (2015). [arXiv:1504.01726](#) [hep-ph]
20. L. Linssen, A. Miyamoto, M. Stanitzki, H. Weerts. [arXiv:1202.5940](#) [physics.ins-det]
21. H. Abramowicz et al., [CLIC Detector and Physics Study Collaboration], Physics at the CLIC  $e^+e^-$  Linear Collider – Input to the Snowmass process 2013. [arXiv:1307.5288](#) [hep-ex]
22. G. Weiglein et al., [LHC/ILC Study Group], *Phys. Rep.* **426**, 47 (2006). [arXiv:hep-ph/0410364](#)
23. A. De Roeck et al., *Eur. Phys. J. C* **66**, 525 (2010). [arXiv:0909.3240](#) [hep-ph]
24. A. De Roeck, J. Ellis, S. Heinemeyer, *CERN Cour.* **49N10**, 27 (2009)
25. S. Heinemeyer, F. von der Pahlen, C. Schappacher, *Eur. Phys. J. C* **72**, 1892 (2012). [arXiv:1112.0760](#) [hep-ph]
26. S. Heinemeyer, F. von der Pahlen, C. Schappacher. [arXiv:1202.0488](#) [hep-ph]
27. A. Bharucha, S. Heinemeyer, F. von der Pahlen, C. Schappacher, *Phys. Rev. D* **86**, 075023 (2012). [arXiv:1208.4106](#) [hep-ph]
28. A. Bharucha, S. Heinemeyer, F. von der Pahlen, *Eur. Phys. J. C* **73**, 2629 (2013). [arXiv:1307.4237](#) [hep-ph]
29. S. Heinemeyer, C. Schappacher, *Eur. Phys. J. C* **75**(5), 230 (2015). [arXiv:1503.02996](#) [hep-ph]
30. A. Bartl, H. Fraas, W. Majerotto, *Z. Phys. C* **30**, 441 (1986)
31. A. Bartl, H. Fraas, W. Majerotto, *Nucl. Phys. B* **278**, 1 (1986)
32. G.J. Gounaris, C. Le Mouél, *Phys. Rev. D* **66**, 055007 (2002). [arXiv:hep-ph/0204152](#)
33. P. Osland, A. Vereshagin, *Phys. Rev. D* **76**, 036001 (2007). [arXiv:0704.2165](#) [hep-ph] [Erratum-ibid. **D 76** (2007) **036001**]
34. K. Rolbieceki, J. Kalinowski, *Phys. Rev. D* **76**, 115006 (2007). [arXiv:0709.2994](#) [hep-ph]
35. P. Osland, J. Kalinowski, K. Rolbieceki, A. Vereshagin. [arXiv:0709.3358](#) [hep-ph]
36. M.A. Díaz, S.F. King, D.A. Ross, *Nucl. Phys. B* **529**, 23 (1998). [arXiv:hep-ph/9711307](#)
37. S. Kiyoura, M.M. Nojiri, D.M. Pierce, Y. Yamada, *Phys. Rev. D* **58**, 075002 (1998). [arXiv:hep-ph/9803210](#)
38. T. Blank, W. Hollik. [arXiv:hep-ph/0011092](#)
39. M.A. Díaz, D.A. Ross. [arXiv:hep-ph/0205257](#)
40. H.K. Dreiner, O. Kittel, U. Langenfeld, *Phys. Rev. D* **74**, 115010 (2006). [arXiv:hep-ph/0610020](#)
41. H.K. Dreiner, O. Kittel, U. Langenfeld, *Eur. Phys. J. C* **54**, 277 (2008). [arXiv:hep-ph/0703009](#)
42. W. Kilian, J. Reuter, T. Robens, *Eur. Phys. J. C* **48**, 389 (2006). [arXiv:hep-ph/0607127](#)
43. T. Robens, Ph.D. thesis, Hamburg, Germany, 2006. [arXiv:hep-ph/0610401](#)
44. T. Blank, Strahlungskorrekturen zur Chargino- und Neutralino-Produktion in  $e^+e^-$  und Hadronkollisionen. Ph.D. thesis, Karlsruhe, Germany (2000)
45. M.A. Díaz, D.A. Ross, *JHEP* **0106**, 001 (2001). [arXiv:hep-ph/0103309](#)
46. W. Öller, H. Eberl, W. Majerotto, *Phys. Lett. B* **590**, 273 (2004). [arXiv:hep-ph/0402134](#)
47. W. Öller, H. Eberl, W. Majerotto, *Phys. Rev. D* **71**, 115002 (2005). [arXiv:hep-ph/0504109](#)
48. T. Fritzsche, W. Hollik, *Nucl. Phys. Proc. Suppl.* **135**, 102 (2004). [arXiv:hep-ph/0407095](#)
49. T. Fritzsche. [arXiv:hep-ph/0408307](#)
50. T. Fritzsche, Ph.D. thesis, Cuvillier-Verlag, Göttingen (2005) (ISBN: 3-86537-577-4)
51. M.A. Díaz, M.A. Rivera, D.A. Ross, *JHEP* **1004**, 098 (2010). [arXiv:0911.4403](#) [hep-ph]
52. A. Bharucha, A. Fowler, G. Moortgat-Pick, G. Weiglein, *JHEP* **1305**, 053 (2013). [arXiv:1211.3134](#) [hep-ph]
53. A. Bharucha, J. Kalinowski, G. Moortgat-Pick, K. Rolbieceki, G. Weiglein, *Eur. Phys. J. C* **73**(6), 2446 (2013). [arXiv:1211.3745](#) [hep-ph]
54. J. Küblbeck, M. Böhm, A. Denner, *Comput. Phys. Commun.* **60**, 165 (1990)
55. T. Hahn, *Comput. Phys. Commun.* **140**, 418 (2001). [arXiv:hep-ph/0012260](#)
56. T. Hahn, C. Schappacher, *Comput. Phys. Commun.* **143**, 54 (2002). [arXiv:hep-ph/0105349](#)
57. Program, user's guide and model files are available via. <http://www.feynarts.de>
58. T. Fritzsche, T. Hahn, S. Heinemeyer, F. von der Pahlen, H. Rzehak, C. Schappacher, *Comput. Phys. Commun.* **185**, 1529 (2014). [arXiv:1309.1692](#) [hep-ph]
59. T. Hahn, M. Pérez-Victoria, *Comput. Phys. Commun.* **118**, 153 (1999). [arXiv:hep-ph/9807565](#)
60. Program and user's guide are available via. <http://www.feynarts.de/formcalc/>
61. S. Heinemeyer, C. Schappacher, *Eur. Phys. J. C* **75**(5), 198 (2015). [arXiv:1410.2787](#) [hep-ph]
62. S. Heinemeyer, H. Rzehak, C. Schappacher, *Phys. Rev. D* **82**, 075010 (2010). [arXiv:1007.0689](#) [hep-ph]
63. S. Heinemeyer, H. Rzehak, C. Schappacher, *PoSCHARGED* **2010**, 039 (2010). [arXiv:1012.4572](#) [hep-ph]
64. T. Fritzsche, S. Heinemeyer, H. Rzehak, C. Schappacher, *Phys. Rev. D* **86**, 035014 (2012). [arXiv:1111.7289](#) [hep-ph]
65. S. Heinemeyer, C. Schappacher, *Eur. Phys. J. C* **72**, 1905 (2012). [arXiv:1112.2830](#) [hep-ph]
66. S. Heinemeyer, C. Schappacher, *Eur. Phys. J. C* **72**, 2136 (2012). [arXiv:1204.4001](#) [hep-ph]
67. S. Heinemeyer, C. Schappacher, *Eur. Phys. J. C* **76**(4), 220 (2016). [arXiv:1511.06002](#) [hep-ph]
68. S. Heinemeyer, C. Schappacher, *Eur. Phys. J. C* **76**(10), 535 (2016). [arXiv:1606.06981](#) [hep-ph]
69. M. Frank, T. Hahn, S. Heinemeyer, W. Hollik, H. Rzehak, G. Weiglein, *JHEP* **0702**, 047 (2007). [arXiv:hep-ph/0611326](#)
70. A. Fowler, Ph.D. thesis: Higher-order and CP-violating effects in the neutralino and Higgs-boson sectors of the MSSM. Durham University, UK, September (2010)
71. A. Fowler, G. Weiglein, *JHEP* **1001**, 108 (2010). [arXiv:0909.5165](#) [hep-ph]
72. A. Chatterjee, M. Drees, S. Kulkarni, Q. Xu, *Phys. Rev. D* **85**, 075013 (2012). [arXiv:1107.5218](#) [hep-ph]
73. A. Denner, S. Dittmaier, M. Roth, D. Wackerroth, *Nucl. Phys. B* **560**, 33 (1999). [arXiv:hep-ph/9904472](#)
74. F. del Aguila, A. Culatti, R. Muñoz-Tapia, M. Pérez-Victoria, *Nucl. Phys. B* **537**, 561 (1999). [arXiv:hep-ph/9806451](#)
75. W. Siegel, *Phys. Lett. B* **84**, 193 (1979)
76. D. Capper, D. Jones, P. van Nieuwenhuizen, *Nucl. Phys. B* **167**, 479 (1980)
77. D. Stöckinger, *JHEP* **0503**, 076 (2005). [arXiv:hep-ph/0503129](#)
78. W. Hollik, D. Stöckinger, *Phys. Lett. B* **634**, 63 (2006). [arXiv:hep-ph/0509298](#)
79. A. Denner, *Fortsch. Phys.* **41**, 307 (1993). [arXiv:0709.1075](#) [hep-ph]
80. K. Fabricius, I. Schmitt, G. Kramer, G. Schierholz, *Zeit. Phys. C* **11**, 315 (1981)
81. G. Kramer, B. Lampe, *Fortschr. Phys.* **37**, 161 (1989)
82. H. Baer, J. Ohnemus, J. Owens, *Phys. Rev. D* **40**, 2844 (1989)



83. B. Harris, J. Owens, Phys. Rev. D **65**, 094032 (2002). [arXiv:hep-ph/0102128](#)
84. T. Hahn, Comput. Phys. Commun. **168**, 78 (2005). [arXiv:hep-ph/0404043](#)
85. T. Hahn. [arXiv:1408.6373](#) [physics.comp-ph]. Available at: <http://www.feynarts.de/cuba/>
86. J. Aguilar-Saavedra et al., Eur. Phys. J. C **46**, 43 (2006). [arXiv:hep-ph/0511344](#)
87. H. Eberl, W. Majerotto, V. Spanos, Phys. Lett. B **538**, 353 (2002). [arXiv:hep-ph/0204280](#)
88. H. Eberl, W. Majerotto, V. Spanos, Nucl. Phys. B **657**, 378 (2003). [arXiv:hep-ph/0210038](#)
89. T. Hahn, S. Heinemeyer, G. Weiglein, Nucl. Phys. B **652**, 229 (2003). [arXiv:hep-ph/0211204](#)
90. T. Hahn, S. Heinemeyer, G. Weiglein, Nucl. Phys. Proc. Suppl. **116**, 336 (2003). [arXiv:hep-ph/0211384](#)
91. A. Bharucha, Private communication, 05.03.2015 and 11.04.2017
92. S. Amoroso, Talk given at “Moriond QCD”, March 2017. See <https://moriond.in2p3.fr/QCD/2017/TuesdayMorning/Amoroso.pdf>. <https://twiki.cern.ch/twiki/bin/view/AtlasPublic/Amoroso.pdf>
93. M. Marionneau, Talk given at “Moriond EWK”, March 2017. See <https://indico.in2p3.fr/event/13763/session/4/contribution/44/material/slides/1.pdf>
94. R. Patel, Talk given at “Moriond QCD”, March 2017. See <https://moriond.in2p3.fr/QCD/2017/TuesdayMorning/Patel.pdf>. <https://twiki.cern.ch/twiki/bin/view/CMSPublic/PhysicsResultsSUS>
95. C. Patrignani et al., [Particle Data Group], Chin. Phys. C **420**, 100001 (2016)
96. J. Frère, D. Jones, S. Raby, Nucl. Phys. B **222**, 11 (1983)
97. M. Claudson, L. Hall, I. Hinchliffe, Nucl. Phys. B **228**, 501 (1983)
98. C. Kounnas, A. Lahanas, D. Nanopoulos, M. Quiros, Nucl. Phys. B **236**, 438 (1984)
99. J. Gunion, H. Haber, M. Sher, Nucl. Phys. B **306**, 1 (1988)
100. J. Casas, A. Lleyda, C. Muñoz, Nucl. Phys. B **471**, 3 (1996). [arXiv:hep-ph/9507294](#)
101. P. Langacker, N. Polonsky, Phys. Rev. D **50**, 2199 (1994). [arXiv:hep-ph/9403306](#)
102. A. Strumia, Nucl. Phys. B **482**, 24 (1996). [arXiv:hep-ph/9604417](#)
103. M. Frank et al., Phys. Rev. D **88**(5), 055013 (2013). [arXiv:1306.1156](#) [hep-ph]
104. S. Dimopoulos, S. Thomas, Nucl. Phys. B **465**, 23 (1996). [arXiv:hep-ph/9510220](#)
105. M. Dugan, B. Grinstein, L. Hall, Nucl. Phys. B **255**, 413 (1985)
106. D. Demir, O. Lebedev, K. Olive, M. Pospelov, A. Ritz, Nucl. Phys. B **680**, 339 (2004). [arXiv:hep-ph/0311314](#)
107. D. Chang, W. Keung, A. Pilaftsis, Phys. Rev. Lett. **82**, 900 (1999). [arXiv:hep-ph/9811202](#) [Erratum-ibid. **83** (1999) 3972]
108. A. Pilaftsis, Phys. Lett. B **471**, 174 (1999). [arXiv:hep-ph/9909485](#)
109. O. Lebedev, K. Olive, M. Pospelov, A. Ritz, Phys. Rev. D **70**, 016003 (2004). [arXiv:hep-ph/0402023](#)
110. W. Hollik, J. Illana, S. Rigolin, D. Stöckinger, Phys. Lett. B **416**, 345 (1998). [arXiv:hep-ph/9707437](#)
111. W. Hollik, J. Illana, S. Rigolin, D. Stöckinger, Phys. Lett. B **425**, 322 (1998). [arXiv:hep-ph/9711322](#)
112. P. Nath, Phys. Rev. Lett. **66**, 2565 (1991)
113. Y. Kizukuri, N. Oshimo, Phys. Rev. D **46**, 3025 (1992)
114. T. Ibrahim, P. Nath, Phys. Lett. B **418**, 98 (1998). [arXiv:hep-ph/9707409](#)
115. T. Ibrahim, P. Nath, Phys. Rev. D **57**, 478 (1998). [arXiv:hep-ph/9708456](#) [Erratum-ibid. **D 58** (1998) 019901; erratum-ibid. **D 60** (1998) 079903; erratum-ibid. **D 60** (1999) 119901]
116. M. Brhlik, G. Good, G. Kane, Phys. Rev. D **59**, 115004 (1999). [arXiv:hep-ph/9810457](#)
117. S. Abel, S. Khalil, O. Lebedev, Nucl. Phys. B **606**, 151 (2001). [arXiv:hep-ph/0103320](#)
118. Y. Li, S. Profumo, M. Ramsey-Musolf, JHEP **1008**, 062 (2010). [arXiv:1006.1440](#) [hep-ph]
119. N. Yamanaka, Phys. Rev. D **87**, 011701 (2013). [arXiv:1211.1808](#) [hep-ph]
120. V. Barger, T. Falk, T. Han, J. Jiang, T. Li, T. Plehn, Phys. Rev. D **64**, 056007 (2001). [arXiv:hep-ph/0101106](#)
121. G. Moortgat-Pick et al., Phys. Rep. **460**, 131 (2008). [arXiv:hep-ph/0507011](#)